Contrib Mineral Petrol (2012) 163:353–378
DOI 10.1007/s00410-011-0676-6

ORIGINAL PAPER

U–Pb zircon dating of the Gruf Complex: disclosing the late Variscan granulitic lower crust of Europe stranded in the Central Alps

A. Galli · B. Le Bayon · M. W. Schmidt · J.-P. Burg · E. Reusser · S. A. Sergeev · A. Larionov

Received: 22 August 2010 / Accepted: 29 July 2011 / Published online: 30 August 2011

Abstract Permian granulites associated with noritic intrusions and websterites are a common feature of the post-Variscan European crust. Such granulites are common in the Southern Alps (e.g. Ivrea Zone), but occur only in the Gruf Complex in the Central Alps. To understand the geotectonic significance of these granulites, in particular in the context of Alpine migmatisation, zircons from 15 high-grade samples have been U–Pb dated by SHRIMP II analysis. Oscillatory zoned zircons from charnockite sheets, interpreted as melts generated through granulite facies fluid-absent biotite melting at 920–940°C, yield ages of 282–260 Ma. Some of these zircons contain inclusions of opx, unequivocally attributable to the granulite facies, thus confirming a Permian age for the charnockites and associated granulites. Two samples from an enclave-rich orthogneiss sheet yield Cambrian and Ordovician zircon cores. Two deformed leucogranites and six ortho- and augengneisses, which compose two-thirds of the Gruf Complex, give zircon ages of 290–260 Ma. Most zircons have milky rims with ages of 34–29 Ma. These rims date the Alpine amphibolite facies migmatisation, an interpretation confirmed by directly dating a leucosome pocket from upper amphibolite facies metapelites. The Gruf charnockites associated with metre-scale schlieren and boudins of opx–sapphirine–garnet–granulites, websterites and gabbronorites can thus be identified as part of the post-Variscan European lower crust. A geotectonic reconstruction reveals that this piece of lower crust stranded in the (European) North upon rifting of the Neotethys, such contrasting the widespread granulite units in the Southern Alps. Emplacement of the Gruf lower crust into its present-day position occurred during migmatisation and formation of the Bergell Pluton in the aftermath of the breakoff of the European slab.

Keywords Gruf Complex · Permian granulites and charnockites · Central Alps

Communicated by T. L. Grove.

Electronic supplementary material The online version of this article (doi:10.1007/s00410-011-0676-6) contains supplementary material, which is available to authorized users.

A. Galli · B. Le Bayon · M. W. Schmidt (✉) · J.-P. Burg · E. Reusser
Department of Earth Sciences, ETH- and University Zurich, 8092 Zurich, Switzerland
e-mail: max.schmidt@erdw.ethz.ch

B. Le Bayon
BRGM, 3 Avenue Claude-Guillemin, BP 36009, 45060 Orléans Cedex 2, France

S. A. Sergeev · A. Larionov
All-Russian Geological Research Institute (VSEGEI), Centre of Isotopic Research, 74 Sredny Prospect, 199106 St.Peterburg, Russia

Introduction

The Gruf Complex (Fig. 1) is unique and pre-eminent in the Central Alps because of its sheets of ultrahigh-temperature (UHT) charnockites and associated schlieren and lenses of sapphirine–opx–garnet granulites (Cornelius 1916; Wenk et al. 1974; Galli et al. 2011). Understanding this high-grade rock association contained in regional, upper amphibolite facies migmatitic orthogneisses is fundamental to decipher the tectono-metamorphic evolution of the Central Alps and, from a more general point of view, to understand the significance of ultrahigh-temperature metamorphism in modern orogenesis. For this purpose, one

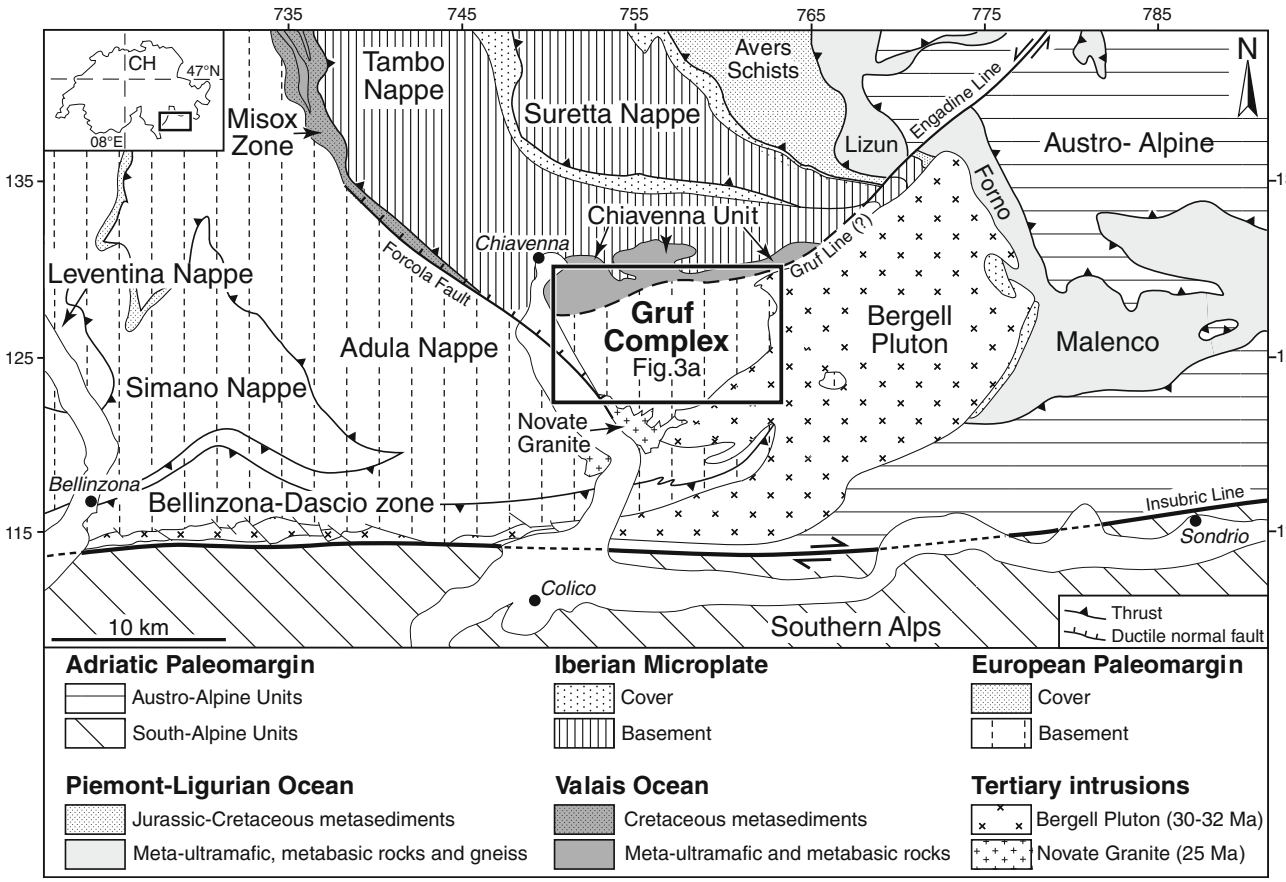

Fig. 1 Simplified tectonic map of the eastern Central Alps with location of the studied Gruf Complex. The main units are listed in legend according to their palaeogeographical origin. *Inset*: Location of the studied area in Switzerland (CH)

relies on accurate geochronological data. U–Pb dating of zircons can record multiple, high temperature geological events (Watson and Harrison 1983; Cherniak and Watson 2003; Hoskin and Schaltegger 2003). Complex zircons are conveniently analysed by the sensitive high-resolution ion microprobe (SHRIMP), which allows the measurement of isotopic ratios of compositional domains imaged with backscattered electrons and cathodoluminescence in single mineral grains (Compston et al. 1992; Hanchar and Miller 1993; De Laeter and Kennedy 1998). We thus carried out SHRIMP isotopic determinations on zircons separated from charnockites and their migmatitic country rocks in the Gruf Complex.

The granulite ultrahigh-temperature peak mineral assemblages comprising, among others, sapphirine, opx, sillimanite, garnet and alkali feldspar formed at temperatures of 920–940°C and pressures of 8.5–9.5 kbar (Fig. 2). The granulites were overprinted and partly re-equilibrated, as documented by cordierite-bearing symplectites and corona textures that formed at 720–740°C and 7–7.5 kbar (Galli et al. 2011). These granulites are typically composed of 60–80% mafic minerals (sapphirine, opx, garnet, Ti-rich biotite; Wenk et al. 1974) and are interpreted as the refractory residue after extraction of considerable amounts of charnockitic melt from a Mg–Al-rich metapelitic precursor (Galli et al. 2011). While the granulite peak conditions are extreme at crustal levels and do not fit any known metamorphic event in the Central Alps, post-peak conditions of 720–740°C leading to partial melting match the generally accepted mid-Tertiary regional metamorphic conditions for this part of the Alps (Bucher-Nurminen and Droop 1983; Burri et al. 2005; Galli et al. 2012). This duality renders the UHT metamorphism a questionable Alpine event.

Oscillatory zoned zircon cores in a strongly residual granulite bolder yielded U–Pb ages of 272 ± 4 Ma (Liati and Gebauer 2003). This age corroborates petrographical similarity with granulites of the European lower crust (e.g. Downes et al. 1990; Costa and Rey 1995) related to post-Variscan extension and also matches other granulite ages from the Southern Alps (see Discussion below). Nevertheless, the Gruf granulites have suffered multiple stages of equilibration (Galli et al. 2011) and zircon zones and monazite ages cannot be unambiguously related to distinct metamorphic or magmatic events. Perhaps because of this ambiguity, an Alpine age has been postulated for the UHT

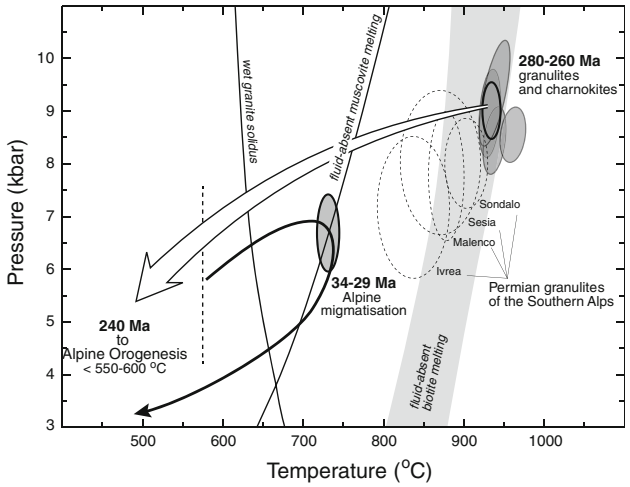

Fig. 2 P–T–t evolution of the granulites and charnockites of the Gruf Complex. Granulite facies P–T conditions (920–940°C, 8.5–9.5 GPa) from Galli et al. (2011). *Grey ellipses* for the 5 granulite types found in the Gruf. Note that the granulite facies conditions agree with the conditions of fluid-absent biotite melting (from Vielzeuf and Holloway 1988; and Stevens et al. 1997). Peak P–T conditions for Southern Alpine granulites: Margna:—Muntener et al. (2000), Sondalo—Braga et al. (2003), Ivrea—Barboza and Bergantz (2000), Sesia—Lardeaux and Spalla (1991), Rebay and Spalla (2001). Garnet diffusion modelling shows that the 282- to 260-Ma granulite event is followed by cooling to less than 550–600°C within 20 Ma (Galli et al. 2011). Whether the granulites were cooled to even lower temperatures (and presumably pressures) cannot be retrieved from garnet diffusion modelling. Pressures and temperatures of the Alpine migmatisation event are determined from cordierite-bearing coronae and symplectites to 720–740°C, 7–7.5 kbar. These conditions are well beyond the wet granite solidus and close to fluid-absent muscovite melting (after Vielzeuf and Schmidt 2001). Our measurements yield ages from 34.3 to 29.2 Ma, and Rubatto et al. (2009) identified a protracted migmatisation lasting from 32 to 22 Ma in the Central Lepontine metamorphic dome

metamorphism by Liati and Gebauer (2003) on the basis of Oligocene U–Pb zircon rim ages (32.7 ± 0.5 Ma) and by Schmitz et al. (2009) on the basis of chemical U–Th–Pb dating of monazite (33 ± 4.4 Ma) from the same residual granulite boulders. All previously investigated granulites were sampled from a talus first described by Cornelius (1916), their direct context remaining unknown. In a previous study (Galli et al. 2011), we have identified the geological context of these granulites and established the existence of large sheets of charnockites (Fig. 1b) that contain schlieren of sapphirine–opx granulites. To elucidate the uncertainty related to dating of zircons in highly restitic granulites, we decided to investigate zircons from the Gruf charnockites as they evidently represent melt formed during the ultrahigh-temperature granulite event (Galli et al. 2011).

The major aims of this study are thus (1) to determine the age of charnockite magmatism and consequently clarify the timing of the UHT granulitic event; (2) to establish the age of regionally widespread partial melting; (3) to assess the protolith age of the migmatitic granitoids and thus establish the timing of crustal growth; and (4) to integrate the dated events of the Gruf Complex into the tectono-metamorphic history of the Central Alps.

Geological setting

The Central Alps (Fig. 1) result from tectonic imbrication of several allochthonous units, the Penninic nappes, stacked during south-dipping subduction of the European plate below the Adrian plate and during subsequent continental collision (Milnes and Pfiffner 1980; Schmid et al. 1996). The regional metamorphic pattern is dominated by Barrovian-type metamorphism (Frey et al. 1974; Frey and Ferreiro Mählmann 1999; Engi et al. 2004). Mineral isograds, isotherms and isobars display a concentric shape and define the 'Lepontine metamorphic Dome' (Wenk 1955; Todd and Engi 1997). This pattern cuts nappe boundaries, showing that peak Barrovian conditions were achieved after nappe thrusting (Niggli and Niggli 1965; Trommsdorff 1966). Metamorphic conditions increase southwards from upper greenschist to upper amphibolite facies and a migmatitic belt near Bellinzona (e.g. Burri et al. 2005). The 32- to 22-Ma migmatisation (Hänny et al. 1975; Köppel et al. 1981; Berger et al. 2009; Rubatto et al. 2009) mainly occurred at 700–750°C and 6–8 kbar (Fig. 2) through fluid-assisted melting and, in a limited amount, fluid-absent muscovite melting (Nagel et al. 2002, Burri et al. 2005; Berger et al. 2008).

The Gruf Complex is located at the eastern end of the Lepontine Dome (Fig. 1). To the north, it is bordered by the ophiolitic Chiavenna Unit and the Tambo Nappe along the putative Gruf Line, described as a vertical, strongly recrystallised mylonite zone (Schmutz 1976). The rocks of the Chiavenna Unit are marked by an isobaric increase in metamorphic temperatures from about 500 to 700°C over less than 3 km (at $P \approx 3$–4 kbar, Schmutz 1976; Talerico 2000). Ar–Ar data suggest that this strong metamorphic gradient formed at 30–33 Ma (Talerico 2000), probably as a result of the rapid, possibly Bergell-related exhumation of the hot Gruf Complex (Bucher-Nurminen and Droop 1983; Talerico 2000). To the east, the Gruf is cut by the calc-alkaline Bergell Pluton, intruded between 33 and 30 Ma (Von Blanckenburg 1992; Oberli et al. 2004; Gregory et al. 2009). To the south, the Gruf Complex is bordered by the 24–25 Ma S-type Novate Granite (Liati et al. 2000). To the west, the Forcola Fault separates the Gruf from the Adula Nappe (Fig. 1).

The Gruf Complex itself (Fig. 3) consists of NNE–SSW-oriented migmatitic biotite-rich orthogneisses, foliated biotite–garnet (±sillimanite ± cordierite) paragneisses and micaschists, sheet-like bodies of charnockites

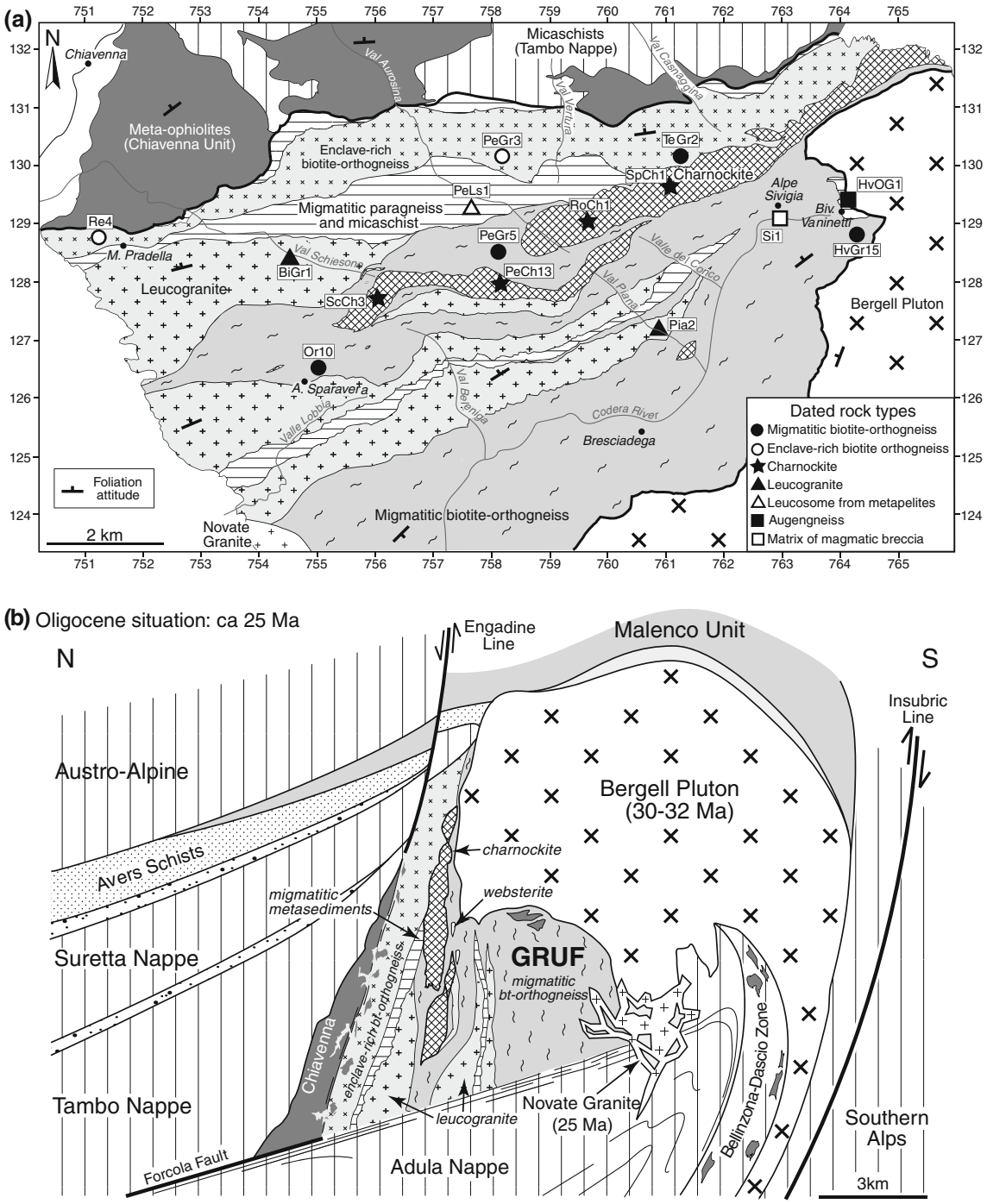

Fig. 3 **a** Location of dated samples in a simplified geological map of the Gruf Complex (Galli et al. 2012). Swiss coordinates are given with units in kilometre. **b** Synthetic profile through the Gruf Complex integrated in the generally accepted section of the southern Central Alps, modified after Schmid et al. (1996), which assumes far-distant projection from east to *top*

containing granulites, and subordinate metamorphosed ultramafic, basic and rarely carbonate lenses within the migmatitic gneisses (e.g. Galli et al. 2012). Previously known only as loose blocks (Cornelius 1916; Wenk et al. 1974), we have documented the outcrops of sapphirine–opx granulites, as rare schlieren within charnockites and as relict enclaves in migmatitic orthogneisses and charnockites (Galli et al. 2011). Formation temperatures of the granulites and charnockites of 920–940°C correspond well to temperatures of biotite-dehydration melting. The association with metre-sized boudins of websterites and gabbronorites (Galli et al. 2011) is characteristic for the European crust of Permian age (e.g. Rey 1993), the gabbronorites (and their websterite cumulates) supplying

additional heat to reach fluid-absent biotite melting temperatures.

Sample description and location

Fifteen samples representing the spectrum of Gruf metagranitoid rocks were selected for dating (Fig. 3a). A summary of field features, mineral assemblages and sample locations is presented in Table 1, Fig. 3a and in the following section. We have shown that the charnockites and the restitic melanocratic granulites (type A–C of Galli et al. 2011) are melt and residue compliments originating through melt extraction from metapelitic sediments. Such a finding is in accordance with previous field studies on igneous charnockites (Kilpatrick and Ellis 1992; Frost et al. 2000) and experimental studies defining melt compositions originating through fluid-absent biotite melting (e.g. Vielzeuf and Holloway 1988). Further evidence for a granulite facies origin of the charnockites derives from metre-long opx–saphirine–garnet-bearing granulite schlieren (type D-F of Galli et al. 2011) contained in the charnockites.

Charnockites (samples ScCh3, PeCh13, RoCh1, SpCh1) constitute sheet-like bodies within migmatitic biotite-orthogneiss. Anastomosing shear zones surround lens-shaped domains with preserved magmatic fabrics, sapphirine–opx-bearing schlieren and disordered networks of cross-cutting leucocratic veins. The leucocratic schlieren contain 3-15% garnet, 3–15% opx, 1–5% sapphirine and 4–36% biotite, the remainder is composed of plagioclase, alkali feldspar and quartz. Geothermobarometry of the schlieren yield results indistinguishable from that of the restitic dark granulites and the charnockites themselves, i.e. 920–940°C, 8.5–9.5 GPa.

The four dated samples were collected from the homogeneous cores of charnockitic lenses (Fig. 4a), where the rock is medium- to coarse-grained, massive and mostly composed of quartz, plagioclase, alkali feldspar, opx, garnet, biotite and ilmenite. Thermobarometric calculations yield crystallisation at 920–940°C and 8.5–9.5 kbar, and the geochemistry of the charnockites (Table 2) is consistent with an origin through fluid-absent biotite melting at these conditions (Galli et al. 2011).

Migmatitic biotite-orthogneisses (samples Or10, PeGr5, TeGr2, HvGr15) constitute the largest part of the Gruf Complex (Fig. 4b). All investigated samples are homogeneous, coarse-grained and mostly constituted of quartz, plagioclase, alkali feldspar and biotite. Sample PeGr5 is almost equigranular (Fig. 4b), samples Or10, TeGr2 and HvGr15 are foliated (4c).

Enclave-rich biotite-orthogneisses (PeGr3, Re4) constitute a 100- to 1,500-m-thick sheet along the northern border of the Gruf Complex (Fig. 3a, b). The matrix orthogneiss is coarse-grained, weakly foliated, mainly composed of quartz, plagioclase, alkali feldspar and coarse-grained biotite. This rock is frequently migmatitic, the leucosomes being distinguished by their non- or weakly foliated texture. The matrix orthogneiss has slightly peraluminous granodioritic compositions (Table 2). The sheet is characterised by centi- to decimetric, internally undeformed, rounded enclaves of mafic composition, which locally may constitute 5–10% of this lithology; on the other extreme, enclaves are only observed every few metres (Fig. 4d). The enclaves, originally mainly composed of plagioclase + amphibole, are heavily overgrown by biotite and are commonly intruded by veinlets of granitic composition. As the orthogneiss forms the northern limit of the Gruf Complex and is in direct contact with the metabasic rocks of the Chiavenna Unit, the enclaves are interpreted to be derived from these mostly metabasalts during the relative uplift of the Gruf Complex with respect to the Chiavenna Unit.

Leucogranites (BiGr1, Pia2) are spatially associated with migmatitic micaschists and paragneisses (Fig. 3a, b). They typically contain m-sized enclaves of metasediments. Sample BiGr1 is fine-grained, weakly foliated and composed of quartz, plagioclase, alkali feldspar, biotite, sillimanite, spinel and millimetric garnet porphyroblasts (Fig. 4e). Sample Pia2 is sub-equigranular, coarse-grained and constituted of quartz, plagioclase, alkali feldspar, biotite, muscovite and garnet. These leucogranites are peraluminous (Table 2).

Leucosome within metapelites (PeLs1) This sample was taken from a leucocratic, 40- to 50-cm-sized melt pocket within sillimanite–garnet–alkali feldspar–biotite migmatitic schists (Fig. 4f). It is interpreted as an in situ melt generated during regional partial melting. The rock is fine- to medium-grained, almost unfoliated and composed of quartz, plagioclase, alkali feldspar, biotite, muscovite and millimetric, rounded garnet porphyroblasts. The occurrence of sillimanite + alkali feldspar and the lack of syn-kinematic muscovite in the host migmatite suggest that melting was induced by the breakdown of muscovite at about 700–750°C (Galli et al. 2011).

*Augengneiss (*sample *HvOG1)* was collected from a ≤20-m-thick sheet within migmatitic metasediments. The augengneiss is slightly foliated, coarse-grained, mainly composed of quartz, plagioclase, alkali feldspar, biotite and muscovite and characterised by centimetric phenocrysts of quartz and feldspar. The sheet displays sharp intrusive contacts with the country rocks (Fig. 4g). Its geochemistry is slightly peraluminous, similar to that of the migmatitic orthogneisses.

Matrix of magmatic breccia (sample Si1) This sample represents the granitic matrix of a breccia (Fig. 4h) characterised by 5–50% rounded, mostly ultramafic but also

Table 1 Main field characteristics, observed mineral assemblage and provenance of the investigated samples

Sample	Rock type				
	Formation	Field characteristics	Mineral assemblage	Swiss coordinates	Altitude (m)
Charnockite					
ScCh3	Orthopyroxene–garnet-bearing melt derived from biotite-dehydration melting of a sedimentary precursor at UHT granulite conditions	8 × 0.5 km large sheet-like bodies within the migmatitic bt-orthogneisses. Internal structure: lense-shaped domains with irregular flow structures, granulitic schlieren and networks of crosscutting melts and dykes separated by anastomosing shear zones. Contact to the country rock: cm mylonites	qtz, pl, ksp, bt, opx, grt, amp, zrc, rut, ilm, opaques	756′056/127′803	2,200
PeCh13			qtz, pl, ksp, bt, opx, grt, amp, chl, spl, zrc, rut, ilm, opaques	758′057/128′116	2,400
RoCh1			qtz, pl, ksp, bt, opx, grt, chl, amp, zrc, rut, ilm, opaques	759′652/129′116	2,350
SpCh1			qtz, pl, ksp, bt, opx, grt, amp, zrc, rut, ilm, opaques	760′869/129592	2,220
Migmatitic bt-orthogneiss					
Or10	Granitoid intrusions	Coarse-grained, slightly foliated	qtz, pl, ksp, bt, ms (rare), chl, ep, ap, zrc, rut/sph, ilm, opaques	755′073/126′380	1,890
HvGr15		Coarse-grained, slightly foliated, with centimetre shear zones	qtz, pl, ksp, bt, chl, ep, ap, zrc, rut/sph, ilm, opaques	764′135/129′063	2,540
TeGr2		Coarse-grained, slightly foliated	qtz, pl, ksp, bt, chl, ep, ap, zrc, rut/sph, ilm, opaques	761′400/130′037	2,240
PeGr5		Coarse-grained, massive	qtz, pl, ksp, bt, chl, amp, ap, zrc, rut/sph, ilm, opaques	758′306/128557	2,200
Enclave-rich bt-orthogneiss					
PeGr3	Granitoid intrusions	Coarse-grained, undeformed with up to 30 cm large, rounded, massive enclaves of mafic composition	qtz, pl, ksp, bt, chl, ep, ap, zrc, rut/sph, ilm, opaques	758′153/129′875	2,015
Re4			qtz, pl, ksp, bt, ep, ap, zrc, rut/sph, ilm, opaques	751′502/128′762	880
Leucogranite					
Pia2	Melt derived by the melting of a pelitic precursor	Coarse-grained and massive	qtz, pl, ksp, bt, grt, sil, ms (rare), zrc, opaques	761′011/127′131	1,750
BiGr1		Fine-grained and slightly foliated	qtz, pl, ksp, bt, ms, grt, sil, spl, zrc, rut/sph, opaques	754′574/128′454	1,315
Leucosome					
PeLs1	Melt derived from muscovite-dehydration melting of pelites	Up to 50 cm large, leucocratic, massive melt pocket discordant to the host migmatitic metapelites	qtz, pl, ksp, bt, ms, grt, sil, spl, zrc, rut/sph, opaques	757′796/129′158	1,890
Augengneiss					
HvOG1	Granitoid intrusion into sedimentary sequence	Coarse-grained, slightly foliated, up to 20-m-thick granitic sheet discordant into migmatitic sediments	qtz, pl, ksp, bt, ms, ep, ap, zrc, rut/sph, opaques	763′960/129′377	2,600
Matrix of magmatic breccia					
Si1	Melt originated by partial melting of a granitoid precursor	Up to 10-cm-thick, leucocratic, massive granitic dykes forming the matrix of a ultramafic breccia	qtz, pl, ksp, bt, grt, ap, zrc, rut/sph, opaques	763′089/128′940	2,080

Mineral abbreviations: qtz, quartz; pl, plagioclase; ksp, alkali feldspar; bt, biotite; ms, muscovite; chl, chlorite; grt, garnet; sil, sillimanite; opx, orthopyroxene; amp, amphibole; spl, spinel; ep, epidote; ap, apatite; zrc, zircon; rut, rutile; sph, sphene; ilm, ilmenite

mafic enclaves (the 'Sivigia-Zug' of Wenk and Cornelius 1977). It is medium- to coarse-grained, almost unfoliated and constituted of quartz, plagioclase, alkali feldspar, biotite and rare, millimetric garnet. Field observations suggest that this breccia (and similar occurrences nearby) formed by injection of leucocratic leucosomes from the migmatitic biotite-orthogneiss into ultramafic lenses and associated metabasic rocks (Galli et al. 2012).

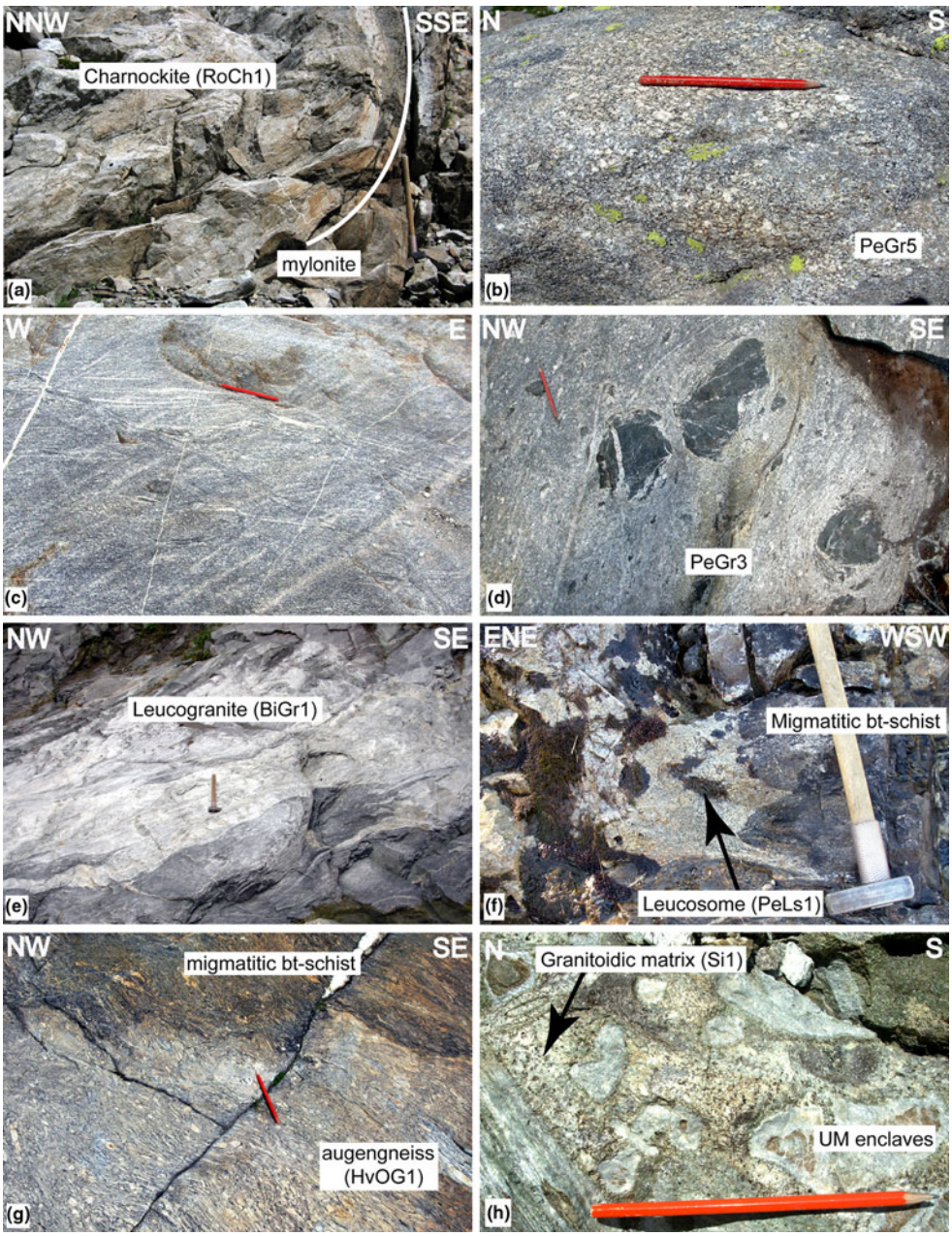

Fig. 4 Field aspect of dated rocks located in Fig. 1b and summarised in Table 1. **a** Homogeneous, coarse-grained and massive lens-shaped domain in RoCh1 charnockite, bounded by centimetre-thick, anastomosing shear zone; **b** massive and coarse-grained biotite-orthogneiss PeGr5; **c** foliated biotite-orthogneiss HvGr15; **d** foliated and coarse-grained PeGr3 biotite-orthogneiss with mafic enclaves; **e** foliated BiGr1 leucogranite; **f** PeLs1 leucosome discordant to the main foliation of the hosting migmatitic biotite-schist; **g** coarse-grained HvOG1 augengneiss (*bottom*) intrusive into migmatitic biotite-schists (*top*); **h** magmatic breccia formed by massive, Si1 leucocratic matrix of granitic composition and rounded components of ultramafic compositions. The components display greyish reaction rims of talc and chlorite

SHRIMP U–Pb geochronology

Analytical technique and data evaluation

More than 1 kg of fresh and homogeneous material was processed for each sample. Zircons were separated at ETH Zurich by standard grinding, Wilfley table, heavy liquids and magnetic separation procedures. The zircons have been cast with Buehler Epokwick resin along with standard zircons 91500 (Wiedenbeck et al. 1995) and Temora (Black et al. 2003). After epoxy-cured (ca. 4–5 days), the puck was polished till zircon grains were half-sectioned. Optic transmitted and reflected light images as well as BSE and CL microphotographs were taken in order to distinguish between different zircon domains and to choose the positions of analytical spots. In situ U–Pb analyses were performed using a SHRIMP II in the Center of Isotopic Research (CIR) at VSEGEI, Saint-Petersbourg, applying a secondary electron multiplier in peak-jumping mode following the procedure described by Williams (1998) and Larionov et al. (2004). The primary O_2^- beam, c. 27 × 20 μm in size, had corresponding currents of 4.5–5.0 nA. The mass-resolution $M/\Delta M \geq 5{,}000$ (1% valley) allowed resolution of possible isobaric interferences.

Four cycles through the following ion species were measured: $^{196}(Zr_2O)$–^{204}Pb–background (c. 204 AMU)–^{206}Pb–

Table 2 Bulk rock compositions (wt%) and zircon saturation levels for the Gruf metagranitoids

Sample	Rock type														
	Charnockite				Migmatitic bt-orthogneiss				Enclave-rich bt-orthogneiss		Leucogranite		Leucosome	Augengneiss	Matrix
	ScCh3	PeCh13	RoCh1	SpCh1	Or10	HvGr15	TeGr2	PeGr5	PeGr3	Re4	Pia2	BiGr1	PeLs1	HvOG1	Si1
SiO_2 (wt%)	61.49	70.37	66.35	65.75	63.66	66.32	66.97	68.75	67.17	70.59	73.17	73.06	74.35	69.41	71.23
TiO_2	0.72	0.33	0.55	0.61	0.72	0.64	0.45	0.45	0.50	0.33	0.25	0.26	0.06	0.61	0.26
Al_2O_3	18.38	14.98	16.21	16.05	17.28	16.20	15.82	15.31	16.27	15.08	14.18	14.84	14.03	14.80	14.52
FeO[a]	5.75	3.12	4.81	5.42	5.06	4.57	3.94	3.50	3.70	2.27	1.93	1.94	0.94	3.58	3.42
MnO	0.07	0.09	0.09	0.11	0.07	0.09	0.07	0.08	0.06	0.05	0.04	0.04	0.03	0.04	0.13
MgO	1.68	0.92	1.56	2.22	1.33	1.89	1.44	1.00	1.50	0.91	0.45	0.44	0.15	1.02	1.25
CaO	4.78	2.68	3.48	3.27	3.73	3.25	3.19	2.83	3.49	2.22	1.46	1.60	1.03	1.64	2.49
Na_2O	4.08	4.01	3.44	3.18	4.34	4.25	3.81	3.72	4.78	3.79	3.24	3.67	3.58	2.68	3.45
K_2O	1.98	1.76	2.70	2.34	2.31	2.11	2.92	3.62	1.63	3.75	4.46	3.56	5.04	5.21	2.16
P_2O_5	0.34	0.11	0.19	0.18	0.26	0.17	0.18	0.16	0.17	0.05	0.20	0.14	0.07	0.12	0.08
Total	99.3	98.4	99.4	99.1	98.7	99.5	98.8	99.4	99.3	99.0	99.4	99.6	99.3	99.1	99.0
Zr (ppm)	322	95	191	150	300	186	131	185	159	188	93	132	44	248	138
Al/(Na + K+2Ca)	1.05	1.12	1.09	1.17	1.05	1.07	1.04	1.01	1.02	1.05	1.11	1.16	1.06	1.14	1.16
M value[b]	1.394	1.039	1.187	1.119	1.266	1.180	1.191	1.161	1.226	1.036	0.896	0.871	0.869	0.936	0.991
% V_{rim} vs. V_{zircon}	25–30	20–25	20–25	20–25	10–15	15–20	35–40	<10	25–30	15–20	15–20	<10	50–55	10–15	10–15
Zr concentrations (ppm) leading to zircon saturation at equilibrium															
700°C	68	52	58	54	64	60	61	62	63	56	51	49	52	52	49
750°C	130	99	112	102	123	115	116	118	99	95	121	108	97	92	100
800°C	234	178	201	184	221	208	209	212	217	194	174	167	180	179	170
900°C	653	497	559	514	615	579	583	591	605	540	486	466	503	498	474
F (%)—degree of melting necessary to dissolve zircon rims in a granitic melt															
700°C	>100	37–46	65–82	56–70	47–70	46–62	75–86	15–30	63–75	50–67	28–37	14–27	42–46	48–72	28–42
750°C	62–74	19–24	34–43	29–37	24–37	24–32	39–45	8–16	40–48	30–40	12–15	6–12	23–25	27–40	14–21
800°C	34–41	11–13	19–24	16–20	14–20	13–18	22–25	4–9	18–22	15–19	8–11	4–8	12–13	14–21	8–12
900°C	12–15	4–5	7–9	6–7	5–7	5–6	8–9	2–3	7–8	5–7	3–4	1–3	4–5	5–7	3–4
Temperature of complete zircon dissolution at equilibrium															
T (°C)	835	756	799	790	837	795	773	791	778	801	755	789	696	837	796

[a] Total iron as FeO

[b] $M = (Na + K + 2 \times Ca)/(Al \times Si)$ after Watson and Harrison (1983)

^{207}Pb–^{208}Pb–^{238}U–^{248}ThO–^{254}UO. Each fifth measurement was carried out on the TEMORA 1 standard. The Pb/U ratios have been normalised relative to the value of 0.0668 for the $^{206}Pb/^{238}U$ ratio of the 416.75 ± 0.24 Ma TEMORA zircon (Black et al. 2003) and hereafter are referred to as 'calibrated $^{206}Pb/^{238}U$'. The 91500 zircon standard, with U-concentration of 81.2 ppm and a $^{206}Pb/^{238}U$ age of 1062 Ma (Wiedenbeck et al. 1995) was applied as the 'U-concentration' standard. Error in TEMORA standard calibration was 0.4%. During this study, the 91500 standard yielded a $^{207}Pb/^{206}Pb$ age of 1,066 ± 7 Ma ($n = 6$).

The collected results have been processed with the SQUID v1.12 (Ludwig 2005a) and ISOPLOT/Ex 3.22 (Ludwig 2005b) software, with decay constants of Steiger and Jäger (1977) and common lead corrected using measured $^{204}Pb/^{206}Pb$ (Stacey and Kramers 1975). The data are presented on concordia (Wetherill 1956) or Tera–Wasserburg diagrams (Tera and Wasserburg 1972). Uncertainties given for individual analyses (ratios and ages) are at the 1σ level; however, the uncertainties in calculated concordia ages are reported at 2σ level.

CL pattern and zircon characteristics

Charnockites CL images show homogeneous and similar zircon populations in the four charnockite samples. Crystals are commonly elongate, prismatic, euhedral to subhedral with rounded outlines (Fig. 5a). They are 180–450 μm long and 70–200 μm wide. They display low to highly luminescent, both oscillatory and planar zoned cores, typical for zircons precipitated during granite crystallisation (Corfu et al. 2003). A few zircon cores of samples RoCh1 and SpCh1 exhibit broad planar banding (Fig. 5a). In ScCh3 and PeCh13, magmatic zircon domains with oscillatory zoning mantle rare xenocrystic cores. Rims around the magmatic zircon domains commonly truncating zoning patterns are characterised by homogeneous and moderate luminescence. Zircons from samples ScCh3 and RoCh1 display well-developed, 20- to 30-μm-wide rims; zircon rims of samples PeCh13 and SpCh1 are <15 μm wide. In general, these rims are slightly thicker at grain terminations (Fig. 5a). These rims are normally interpreted as metamorphic growths that may or may not have involved melts of migmatitic origin.

Migmatitic biotite-orthogneiss All samples exhibit homogeneous zircon populations of elongate, prismatic grains. Zircons from samples Or10, PeGr5 and HvGr15 are euhedral to subhedral with slightly rounded outlines, while zircons from sample TeGr2 are euhedral with straight edges and sharp angles (Fig. 5b). Grain size varies between 250–600 μm in length and 100–200 μm in width. Cores are dominated by well-developed oscillatory zoning with variable luminescence, interpreted as magmatic in origin. A few crystal cores in samples Or10 and PeGr5 display sector and broad planar zoning. Regular zoning is commonly truncated or resorbed and subsequently overgrown by growth-zoned domains. Rare xenocrystic inner cores are observed in PeGr5 and HvGr15. The volumetrically dominant oscillatory zoned cores are surrounded and truncated by homogeneous rims of variable thickness. These rims become strongly luminescent within 5 μm of their edge. Zircons from sample Or10 show <5-μm-thin rims; rims are 15–20 μm wide in PeGr5 and HvGr15. Rims in TeGr2 are well developed and show weak oscillatory and sector zoning. In some grains, the rims partly replace the oscillatory cores (Fig. 5b).

Enclave-rich biotite-orthogneiss Zircon populations from both samples (PeGr3, Re4) are homogeneous and comprise elongate, prismatic, euhedral crystals with straight edges and sharp angles (Fig. 5c), typically 250–600 μm long and 100–170 μm wide. Crystal cores are weakly to highly luminescent and exhibit oscillatory zoning or, in rare cases, sector zoning typical for zircons of granitic origin. Inherited xenocrystic cores were not found. The oscillatory zoned cores are truncated by ~25- to 30-μm-thick rims, thickest at grain terminations (≤80 μm). Rims are heterogeneous and usually marked by oscillatory, concentric or broad planar zoning, often discordant to the zoning of the grain cores. Some zircon rims have homogeneous, moderately luminescent inner parts surrounded by a thin (<5–10 μm) highly luminescent outermost domain, similar to the zircon rims of sample TeGr2.

Leucogranite Zircons from both samples are elongate to equant, prismatic and euhedral to subhedral with slightly rounded outlines (Fig. 5d). Grains are 150–550 μm long and 75–150 μm wide. In both samples, some zircon cores exhibit a regular oscillatory zoning, whereas others show large, highly luminescent sector-zoned domains surrounded by a thinner, less luminescent oscillatory zoning. No inherited xenocrystic zircons were observed. Zircons in sample BiGr1 have thin (<3–4 μm) or no rims. Zircons in sample Pia2 display moderately luminescent, 20- to 25-μm-wide rims that are thicker (up to 70 μm) at grain terminations.

Leucosome within metapelites Zircon crystals in sample PeLs1 are elongate, prismatic, euhedral to subhedral with slightly rounded outlines (Fig. 5e). They are 200–300 μm long and 75–100 μm wide. Crystal cores are usually moderate to highly luminescent and display oscillatory, sector or broad planar zoning. Rare xenocrystic inner cores were observed. The oscillatory cores are surrounded by homogeneous, bright rims up to 25 μm thick. One zircon is characterised by a bright, homogeneous CL intensity (Fig. 5e). We interpret this single crystal pattern as due to complete re-homogenisation during metamorphism/anatexis.

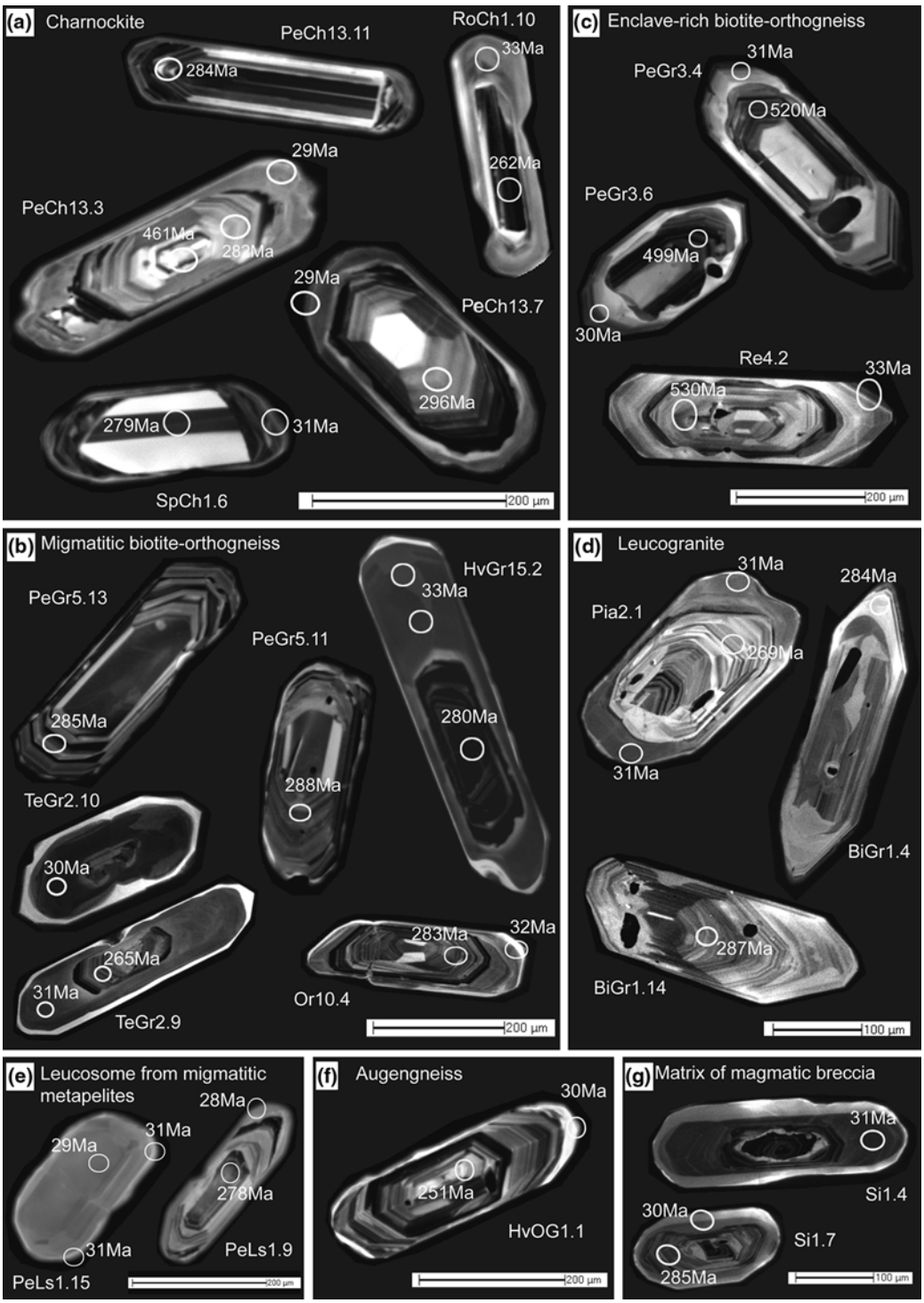

Fig. 5 Cathodoluminescence (*CL*) pictures of representative zircon crystals from metagranitoids of the Gruf Complex. **a** Zircons from charnockites characterised by Permian oscillatory, sector or planar zoned cores and homogeneous, metamorphic outer rims of Alpine age; **b** zircons from migmatitic biotite-orthogneisses displaying oscillatory zoned Permian cores and variably developed and generally homogeneous Alpine metamorphic rims. TeGr2, zircon rim with sector and oscillatory zoning; **c** zircons from the enclave-rich biotite-orthogneiss having both Cambrian and Ordovician oscillatory zoned cores. Grains characterised by thick, oscillatory zoned metamorphic rims, suggesting recrystallisation during partial melting; **d** sector and oscillatory zoned cores and thin metamorphic rims of Alpine age in zircon crystals of leucogranites; **e** zircons from leucosome in metapelites with oscillatory zoned cores and thick metamorphic rims. Left grain completely recrystallised at ca. 30 Ma; **f** zircon from the augengneiss with a well-developed, Permian oscillatory zoning. Alpine rim almost absent; **g** zircon from the leucocratic matrix of the magmatic breccia with Permian oscillatory zoned cores and thick metamorphic rims displaying oscillatory or sector zoning

Table 3 SHRIMP ages for the metagranitoid rocks of the Gruf Complex

Sample	Core age(s) (Ma)[a]	Rim age (Ma)
Charnokites		
ScCh3	260 ± 3	30.63 ± 0.92[b]
PeCh13	282 ± 2	29.17 ± 0.25[b]
RoCh1	260.8 ± 2.1	34.29 ± 0.77[b]
SpCh1	279.5 ± 2.6	30.6 ± 1.2[b]
Migmatitic biotite-orthogneiss		
Or10	287.0 ± 6.1	32.2 ± 0.82[b]
HvGr15	280.3 ± 1.4	32.3 ± 1.8[b]
TeGr2	266.4 ± 1.9	30.46 ± 0.28[c]
PeGr5	287.3 ± 3	No measurable rim
Enclave-rich biotite-orthogneiss		
PeGr3	513.3 ± 7.5–453.0 ± 8.4	30.92 ± 0.67[c]
Re4	530 ± 14–470 290.4 ± 8.1	32.19 ± 0.53[c]
Leucogranites		
Pia2	294 ± 4–265 ± 2	30.86 ± 0.31[b]
BiGr1	288 ± 2	No measurable rim
Leucosome from migmatitic metapelites		
PeLs1	Scattering between 538 and 172 Ma	30.06 ± 0.93[b]
Augengneiss		
HvOG1	260.1 ± 4.0	No rim
Matrix of magmatic breccia ('Siviggia Zug')		
Si1	285.6 ± 3.3	30.61 ± 0.33[c]

Ages are given as weighted mean age with errors at the 95% confidence level

[a] Magmatic age of oscillatory zoned zircon cores

[b] Homogeneous outer zircon rims

[c] Rims display oscillatory zoning

Augengneiss CL images show a homogeneous zircon population (sample HvOG1), characterised by elongate, prismatic, euhedral grains with slightly rounded outlines (Fig. 5f). Crystal sizes are 250–500 μm in length and 100–150 μm in width. Zircons present moderate to highly luminescent oscillatory zoned cores representing granite crystallisation. Grain cores rarely display sector zoning. Xenocrystic inheritance was not found. Thin (<5 μm), homogeneous and highly luminescent rims truncate zoning of the magmatic inner domains.

Matrix of magmatic breccia Zircons in sample Si1 are elongate to equant, euhedral to subhedral with slightly rounded outlines (Fig. 5g). Their length varies from 200 to 600 μm and their width from 75 to 150 μm. CL images revealed cores with moderate luminescence and magmatic oscillatory or, in rare cases, sector zoning. A few grains display xenocrystic inner cores. The oscillatory cores are surrounded by discordant, moderately luminescent rims with a highly luminescent outermost fringe. Rim thicknesses vary considerably from grain to grain. Some rim domains show similar oscillatory patterns as the cores, preserved as ghost oscillatory zoning (Fig. 5g).

In summary, zircons have rare xenocrystic cores and wide, volumetrically dominant outer cores characterised by oscillatory and sector zoning; these are attributed to zircon growth during crystallisation of the granitic host rocks. Most outer zircon rims are milky and attributed to metamorphic recrystallisation possibly involving migmatitic melts. Nevertheless, the migmatitic biotite-orthogneisses TeGr2, the enclave-rich biotite-orthogneiss sheet and the granitic matrix of the magmatic breccia developed broad rims with oscillatory zoning. These rims point to significant partial melting of these three host granites during regional anatexis.

U–Pb results

After the SHRIMP measurements, the exact locations of the single analysis spots were verified by CL imaging to exclude analyses mixing different zircon domains. Results are summarised in Table 3.

Charnockites

ScCh3 Eight data points were obtained from the oscillatory zoned cores of seven zircon grains. Th/U ratios vary between 0.34 and 0.65. One spot yielded an Ordovician age of 478 Ma and seven analyses yielded Permo–Triassic ages of 298–245 Ma. On a Concordia diagram, 3 spots yielded concordant ages of 260 ± 3 Ma (Fig. 6a). Ten spots from the homogeneous rims of ten zircon crystals were measured, but post-SHRIMP CL imaging revealed that four spots touch the oscillatory zoned cores and therefore yield mixed ages. The remaining six have Th/U ratios between

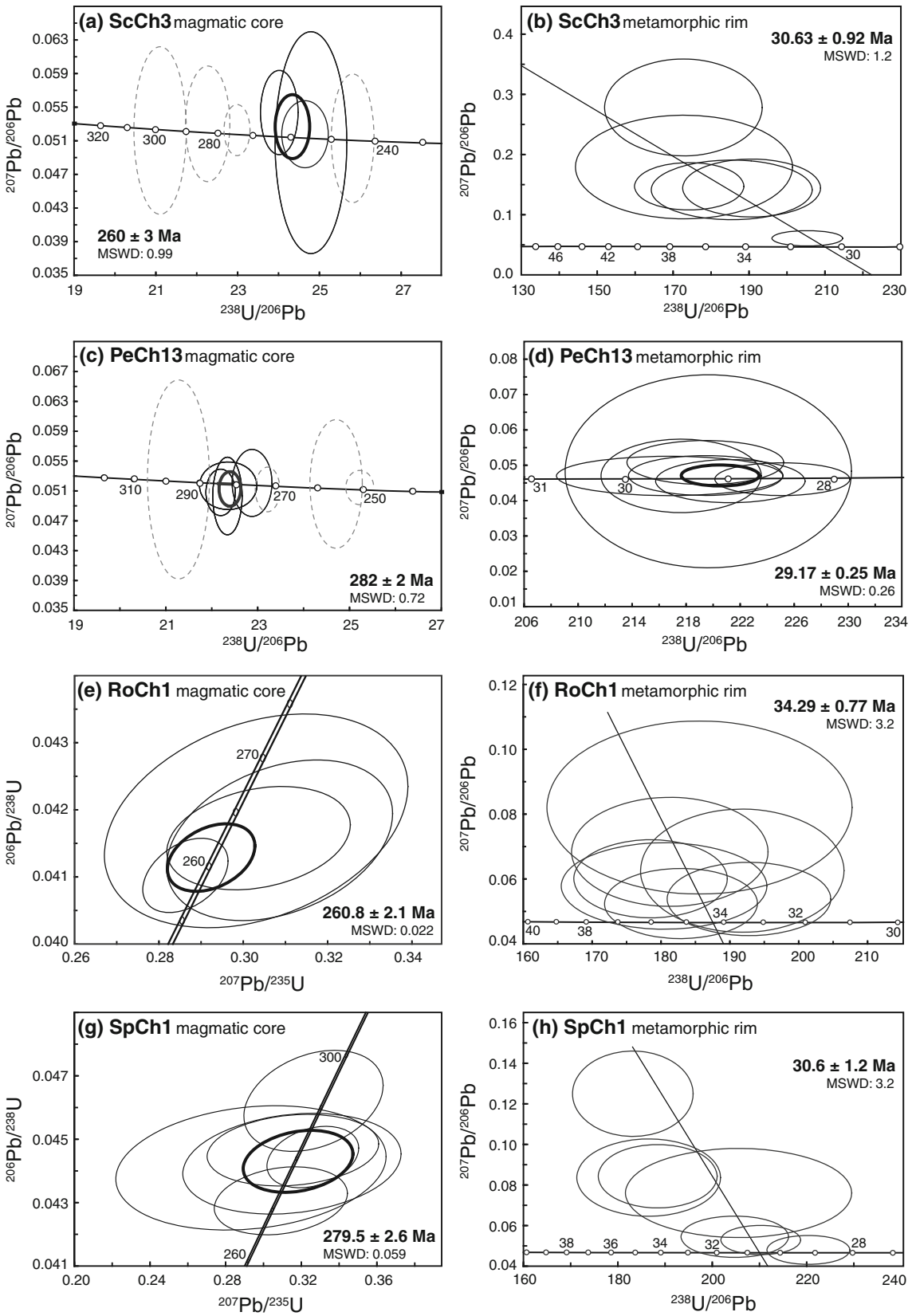

Fig. 6 Concordia and Tera–Wasserburg diagrams with data of zircons separated from the Gruf charnockites. Ages calculated as weighted mean and errors at the 95% confidence level. Ellipses plotted with a 2σ error. Thin, *solid ellipses* concordant ages; *dashed grey ellipses* non-concordant ages, not used for mean age calculation; *bold ellipses* calculated average age

0.02 and 0.44. On a Tera–Wasserburg diagram, they plot on a mixing line between common Pb and calibrated total $^{238}U/^{206}Pb$, intersecting the concordia at a weighted mean age of 30.63 ± 0.92 Ma (Fig. 6b).

PeCh13 Twelve data points were obtained from the oscillatory zoned cores of twelve zircon grains. For these, Th/U ratios vary from 0.14 to 0.96. One spot yielded a Carboniferous age of 305 Ma, nine analyses Permo-Triassic ages between 296 and 247 Ma, and two spots yielded 193 and 131 Ma, respectively (Fig. 6c). On a Concordia diagram, a cluster of four analyses gives a concordant age of 282 ± 2 Ma. Seven spots from homogeneous rims of seven grains yield Th/U ratios of 0.01–0.04. On the Tera–Wasserburg diagram, they plot on the concordia, giving a weighted mean age of 29.17 ± 0.25 Ma (Fig. 6d).

RoCh1 Eleven oscillatory zoned cores of eleven grains were analysed. Their Th/U ratios vary between 0.15 and 1.25. All points yield Carboniferous to Triassic ages, between 310 and 212 Ma. On a Concordia diagram, a cluster of four measurements gives a concordant age of 260.8 ± 2.1 Ma (Fig. 6e). Two out of ten homogeneous rim analyses from ten grains were mixed. The remainder gave Th/U ratios of 0.02–0.35. On a Tera–Wasserburg diagram, seven of them plot on a mixing line between common Pb and calibrated total $^{238}U/^{206}Pb$ (Fig. 6f), intersecting the Concordia at a weighted mean age of 34.29 ± 0.77 Ma.

SpCh1 Nine oscillatory zoned cores were measured, yielding Th/U ratios between 0.16 and 0.78. Six spots gave concordant ages of 279.5 ± 2.6 Ma (Fig. 6g), one analysis (SpCh1.7.1.) yielded an older age of 314.7 ± 3.3 Ma. Post-analysis CL imaging revealed that this latter spot spans a crack, where accumulation of radiogenic Pb may have led to the slightly higher age. Two analyses yielded younger ages, probably due to partial Pb loss after crystallisation. Ten spots were measured in the outer rims of nine grains, but post-analysis CL imaging revealed three mixed analyses. The other seven gave Th/U ratios of 0.01–0.05, and on the Tera–Wasserburg diagram, they lie on a mixing line between common Pb and calibrated total $^{238}U/^{206}Pb$, intersecting the Concordia at a weighted mean age of 30.6 ± 1.2 Ma (Fig. 6h).

Migmatitic biotite-orthogneiss

Or10 Nine spot analyses of oscillatory zoned cores from nine zircon crystals yield Th/U ratios of 0.19–0.62 and Permo-Triassic ages between 291.3 and 245.6 Ma (Fig. 7a). Five are concordant and give an age of 287.0 ± 6.1 Ma. Ten homogeneous rims were analysed but two were mixed. The Th/U ratios range between 0.01 and 0.07 and the eight valid spots yielded a concordant age of 32.20 ± 0.82 Ma (Fig. 7b).

HvGr15 Twelve spot analyses of oscillatory zoned cores display Th/U ratios of 0.10–0.63 and yield Carboniferous to Triassic ages ranging from 320 to 245 Ma. Six of them give a concordant age of 280 ± 3 Ma (Fig. 7c). Two analyses of xenocryst cores yielded an Ordovician age of 482 Ma and a Devonian age of 389 Ma, respectively. Thirteen homogeneous outer rims were analysed but eight of them were mixed. The other five have Th/U ratios of 0.01–0.16 and yield a metamorphic age of 32.3 ± 1.8 Ma (Fig. 7d).

TeGr2 Eight oscillatory zoned cores from eight zircon grains yield Th/U ratios of 0.18–0.44. Five of them give a concordant age of 266.4 ± 1.9 Ma (Fig. 7e). One spot analysis (TeGr2.1.3) yielded a higher age of ~290 Ma. This analysis was not taken into account for the average age because of its high U content of 2,343 ppm, which may lead to erroneous high ages (Mc Laren et al. 1994; Williams et al. 1996). Two other analyses yielded slightly younger ages probably due to post-crystallisation Pb loss. Twelve analyses of the thick outer rims were obtained, eleven of them yielding a low Th/U ratio of 0.01–0.04 and a concordant age of 30.46 ± 0.28 Ma (Fig. 7f). One analysis gave a slightly higher age of ~36 Ma. CL imaging of this spot revealed ghost textures of the oscillatory zoning, which may induce mixed isotopic ages.

PeGr5 Twelve oscillatory zoned cores of twelve different grains with Th/U ratios of 0.02–0.47 were analysed. Ten of them yield a concordant age of 287 ± 3 Ma (Fig. 7g). One analysis gave 305 Ma but was not counted for the average age because of its high (2,577 ppm) U content. One spot analysis yielded a slightly younger Triassic age probably due to post-crystallisation Pb loss. Metamorphic outer rims were too thin to be measured by SHRIMP.

Enclave-rich biotite-orthogneiss

PeGr3 Ten data points were obtained from oscillatory zoned cores of nine zircons with Th/U ratios between 0.12 and 0.18. Two sets of ages have been identified. Five spots yield a concordant Cambrian age of 513.3 ± 7.5 Ma, and four yield a concordant Ordovician age of 453.0 ± 8.4 Ma (Fig. 8a). Thirteen spot analyses were carried out on the wide oscillatory zoned rims of nine crystals yielding variable Th/U ratios of 0.01–0.18. All of them plot on a mixing line between common Pb and calibrated total $^{238}U/^{206}Pb$, intersecting the Concordia at a weighted mean age of 30.92 ± 0.67 Ma (Fig. 8b).

Re4 Nine oscillatory zoned cores from nine zircon grains give Th/U ratios of 0.04–0.79. One data point yielded a Cambrian age of 530 ± 20 Ma, two points yielded Ordovician ages of 464 and 473 Ma, while six points yielded Permian ages between 224 and 300 Ma (Fig. 8c). A cluster of three spots yielded a concordant age of 290.4 ± 8.1 Ma. Twelve

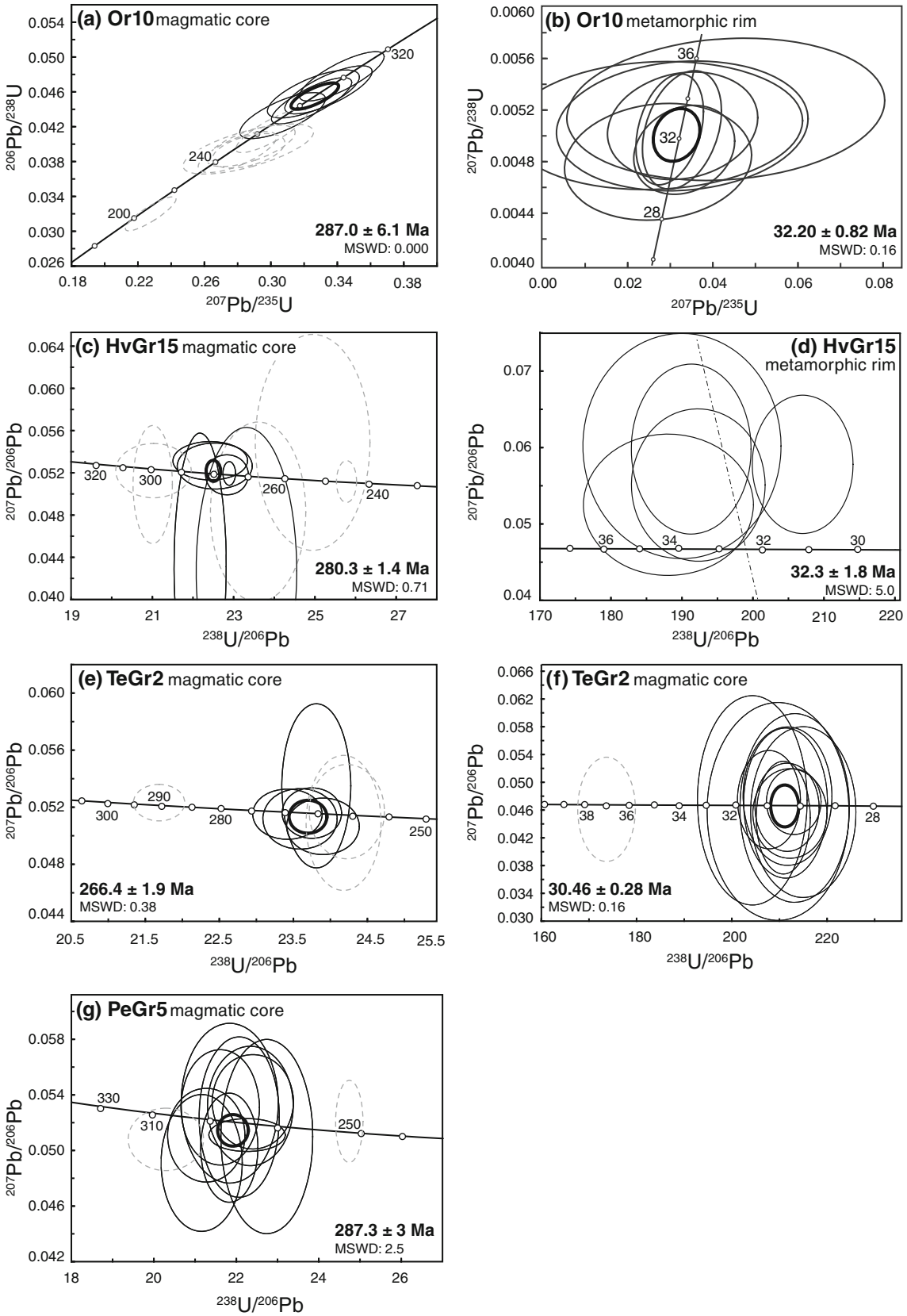

Fig. 7 Concordia and Tera–Wasserburg diagrams with data of zircons separated from the Gruf migmatitic biotite-orthogneisses. Legend and calculation details as for Fig. 6

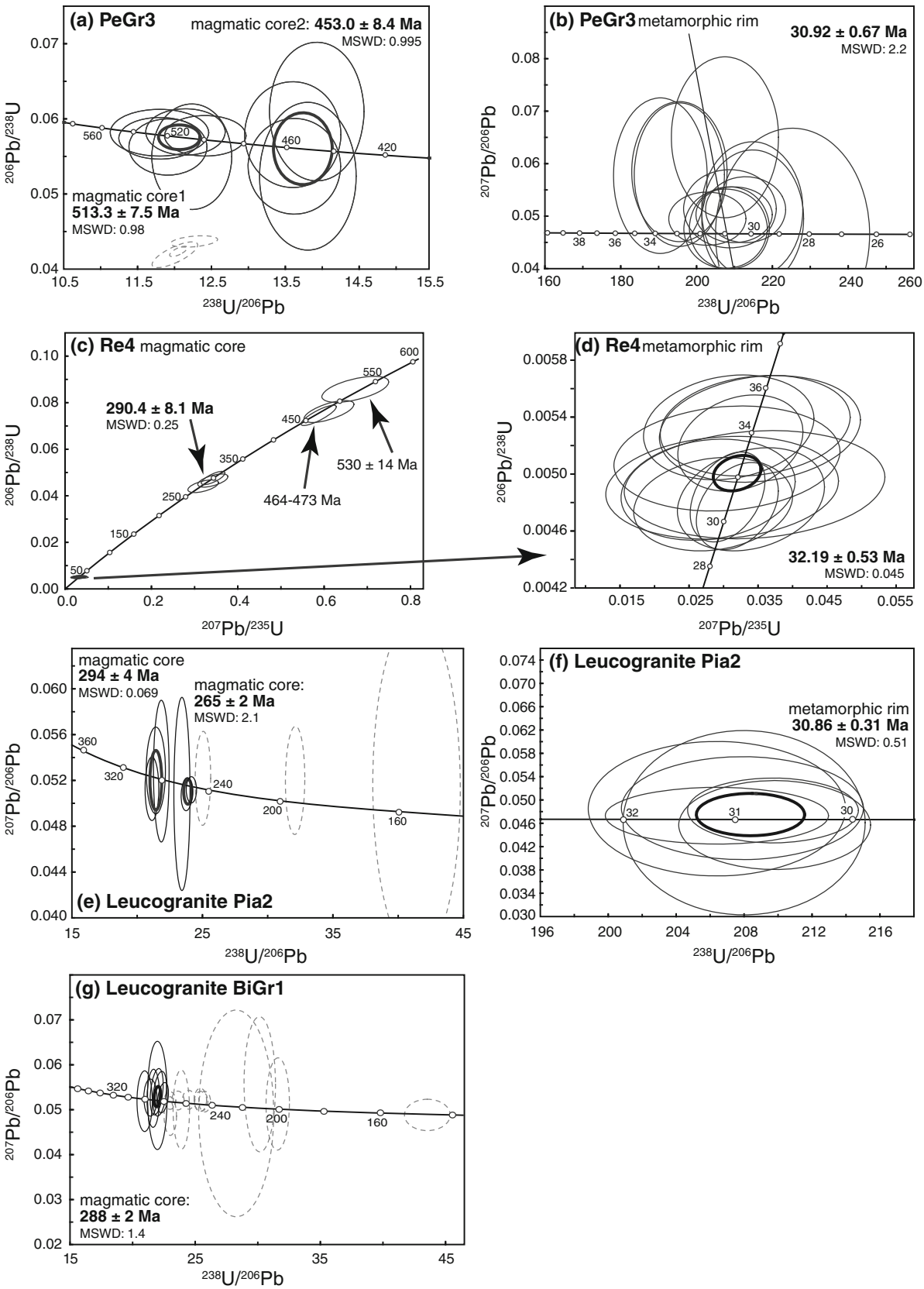

Fig. 8 Concordia and Tera–Wasserburg diagrams with data of zircons separated from the Gruf enclave-rich biotite-orthogneisses (**a**–**d**) and leucogranites (**e**–**g**). Legend and calculation details as for Fig. 6

points in the oscillatory zoned rims of eleven zircon crystals, with Th/U ratio of 0.01–0.20, give a concordant age of 32.19 ± 0.53 Ma (Fig. 8d).

Leucogranite

Pia2 Ten analyses of oscillatory and sector-zoned cores from nine zircon grains give variable Th/U ratios of 0.01–0.45 and Permo-Triassic ages of 153–298 Ma (Fig. 8e). No systematic difference between oscillatory and sector zoning was observed. Three spots yield a concordant age of 293.9 ± 0.3.8 Ma. The broad scattering of the other data likely results from extensive post-crystallisation Pb loss. Eight homogeneous rims were analysed giving Th/U ratios <0.01. Six data points yield a concordant age of 30.86 ± 0.31 Ma (Fig. 8f). The other two were identified as mixed analyses during CL imaging.

BiGr1 Twenty data points were obtained from oscillatory and sector-zoned cores of fifteen grains. Th/U ratios vary between 0.01 and 0.67 and ages are scattered between 300 and 146 Ma (Fig. 8g). A cluster of seven ages yield a concordant age of 288 ± 2 Ma. Rims were too thin (<3–4 μm) to obtain an age.

Leucosome from migmatitic metapelites

PeLs1 Twelve oscillatory and sector-zoned core spots with Th/U ratios of 0.01–0.83 yield ages between 538 Ma and 172 Ma (Fig. 9a). No preferred age is obtained for the oscillatory zoned cores of presumably magmatic origin, consistent with a detrital zircon component in the protolith sediment. Three rim data points out of fifteen were mixed. Twelve yield Th/U ratios of 0.01–0.19 and plot on a mixing line between common Pb and calibrated total $^{238}U/^{206}Pb$, intersecting the Concordia at a weighted mean age of 30.06 ± 0.93 Ma (Fig. 9b). The same age was calculated from the completely re-homogenised grain (Fig. 5e), suggesting that 30.06 ± 0.93 Ma effectively dates partial melting.

Augengneiss

HvOG1 Ten spots were investigated from the oscillatory zoned cores of ten crystals. The measured Th/U ratios range between 0.05 and 0.28. On a Concordia diagram, seven measurements yield a concordant age of 260.1 ± 4 Ma (Fig. 9c). No age could be obtained from the <5-μm-wide rims.

Matrix of magmatic breccia

Si1 Six oscillatory zoned inner cores of six zircon grains have Th/U ratios of 0.21–0.55 and ages scattering between 286 and 220 Ma. Two data points (Si1.5.2 and Si1.7.2) yield a concordant age of 285.6 ± 3.3 Ma (Fig. 9d). Fourteen spots were measured in rims, but four were sampling both oscillatory zoned domains and metamorphic outer rims. The remainder yields Th/U ratios of 0.01–0.51 and concordant ages of 30.61 ± 0.33 Ma (Fig. 9e).

Discussion: formation conditions of zircon domains

Oscillatory zoning in zircons is normally attributed to growth during magma crystallisation (Corfu et al. 2003). To add plausibility that the oscillatory or sector-zoned zircons did crystallise during the intrusion of their host rock, we evaluate whether the host melt could have carried all Zr contained in the specific oscillatory zones in solution. Similarly, the amount of zircon stored in the rims allows calculating the minimal melt fraction necessary to dissolve and reprecipitate these rims (assuming that at >700°C, fluids would lead to melting). Zircons do only in part derive through equilibrium processes. Nevertheless, as discussed below, complete dissolution of the zircons in most of the dated rocks would occur at equilibrium at 100–200°C below the expected intrusion temperatures and in particular the thermobarometrically derived charnockite crystallisation temperature. Further support for a Permian granulite facies derives from mineral inclusions in the Permian oscillatory zircon cores.

Mineral inclusions in charnockite zircons

Most minerals of the charnockite matrix, i.e. quartz, plagioclase, K-feldspar, Ti–rich biotite, garnet, opx and apatite, are also found included within the Permian zircon cores, which are oscillatory, sector or planar zoned. Most relevant Permian zircon cores of samples SpCh1 (Fig. 10a, b), RoCh1 (Figs. 10c and d) and ScCh3 contain 10- to 30-μm-long alumina-rich opx grains., and three of the four analysed opx grains have compositions equivalent to cores of opx in the charnockite matrix with ~4 wt% Al_2O_3, and one, a rim composition with 8.5 wt% Al_2O_3 (electronic appendix). The measured garnet inclusion is within the compositional range of the little zoned garnets in the charnockites. We thus conclude that granulite facies conditions reigned when the zircon cores grew.

Zircon dissolution during melting: age of the granulite facies metamorphism

Investigation of the crystal morphology coupled with U–Pb analyses revealed the composite nature of the studied zircon grains. They all have inherited, oscillatory and/or sector-zoned cores and homogeneous rims. Due to its low

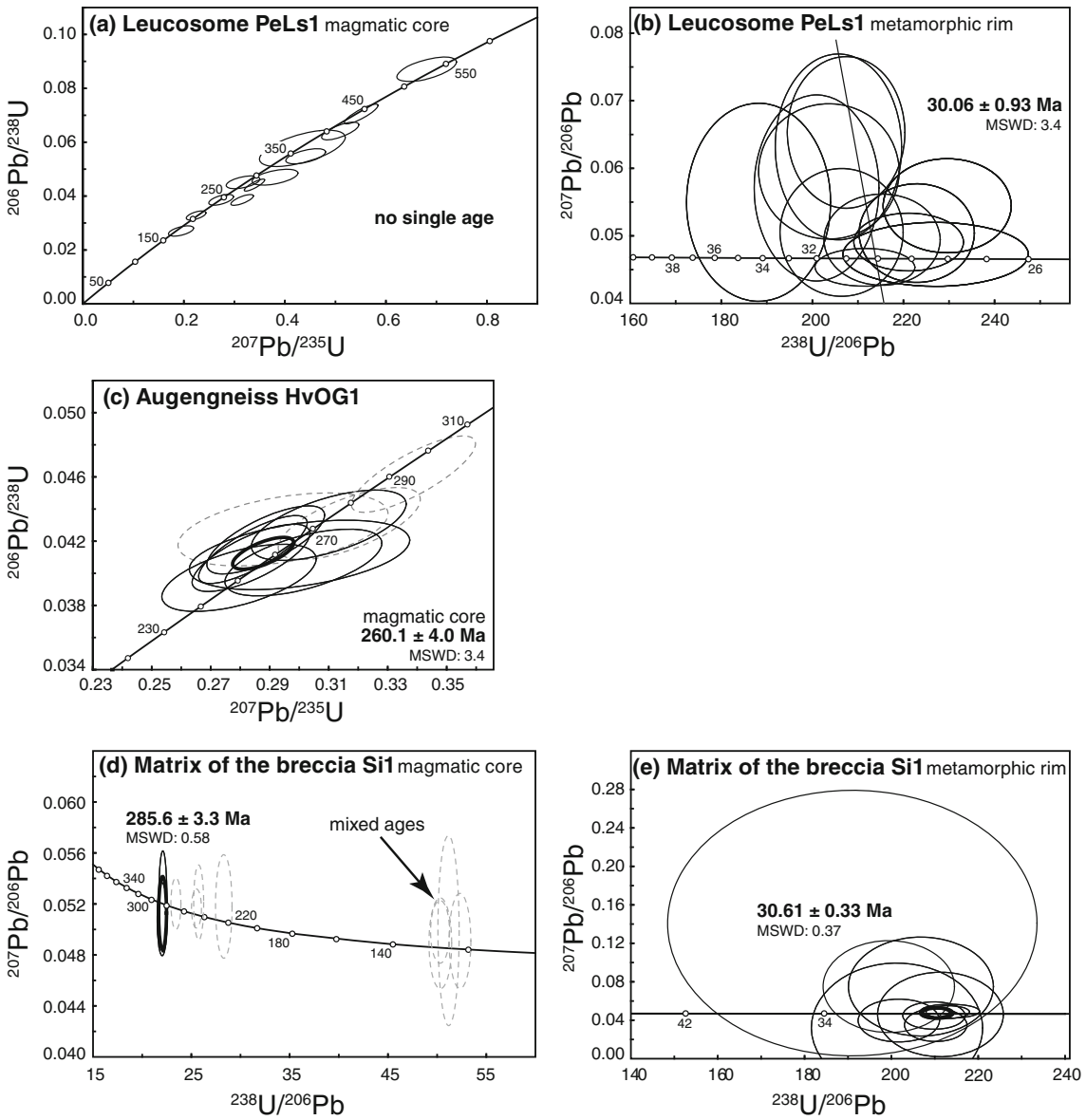

Fig. 9 Concordia and Tera–Wasserburg diagrams with data of zircons separated from the Gruf granitic leucosome (**a**, **b**) augengneiss (**c**) and matrix of a magmatic breccia (**d**, **e**). Legend and calculation details as for Fig. 6

solubility in crustal melts (Watson 1979; Watson and Harrison 1983; Tole 1985), zircons from amphibolite facies migmatitic rocks are commonly only partly dissolved and thus retain at least in part their isotopic inheritance (e.g. Paterson et al. 1992; Watson 1996; Oliver et al. 1999). The major factors controlling Zr solubility in a melt are bulk-rock composition and temperature:

$$\mathrm{Zr}^{\mathrm{melt}}(\mathrm{ppm}) = 5 \times 10^5 \times \exp[3.80 + 0.85 \times (M-1) - (12900/T)],$$

where T is the absolute temperature and M the cationic ratio (Na + K + 2Ca)/(Al × Si) (Watson and Harrison 1983). Using this expression, we calculated the temperature at which complete zircon dissolution would occur at equilibrium and the concentrations of Zr required for zircon saturation of our samples at 700, 750, 800 and 900°C. By 3-dimensional modelling, we then calculated the ratio $V^{\mathrm{rim}}_{\mathrm{zircon}}/V^{\mathrm{total}}_{\mathrm{zircon}}$ to quantify the amount of Zr hosted in zircon rims. XRF bulk-rock data, Zr concentrations, *M* values and the results of our calculations are given in Table 2.

These calculations show that, for the granitic melt compositions of the investigated samples, zircon could completely dissolve between 750 and 840°C, the leucosome excepted, for which zircon could completely dissolve at 700°C (Fig. 11, Table 2). Zircon dissolution during prograde melting is not an equilibrium process. However, the solubility data and relative volumes of cores and rims corroborate critical conclusions. In particular, the charnockites formed at >900°C and thus all of

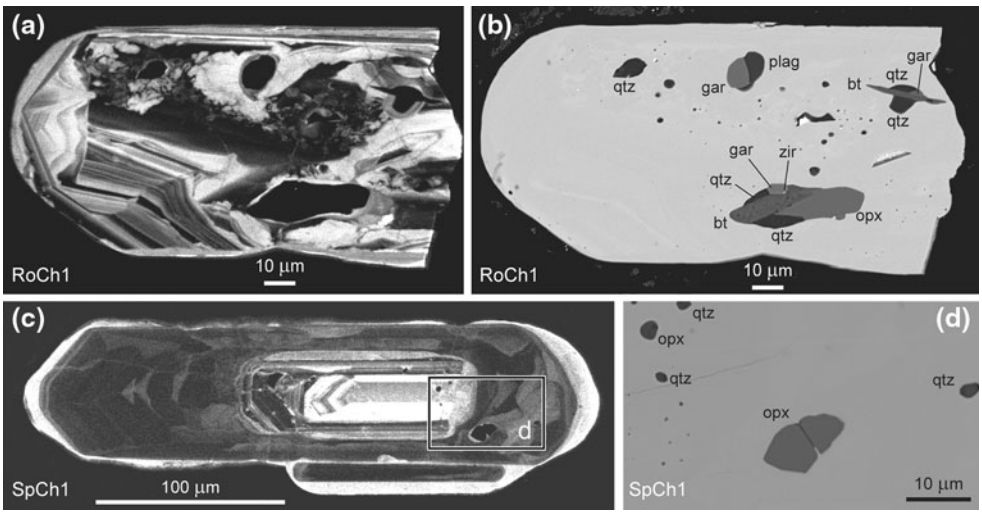

Fig. 10 Cathodoluminescence (**a**, **c**) and BSE (**b**, **d**) images of zircon grains separated from the SpCh1 and RoCh1 charnockites of the Gruf Complex. Opx and garnet grains included within the oscillatory and sector-zoned zircon cores of Permian age demonstrate that the charnockitic mineral assemblage formed in Permian time

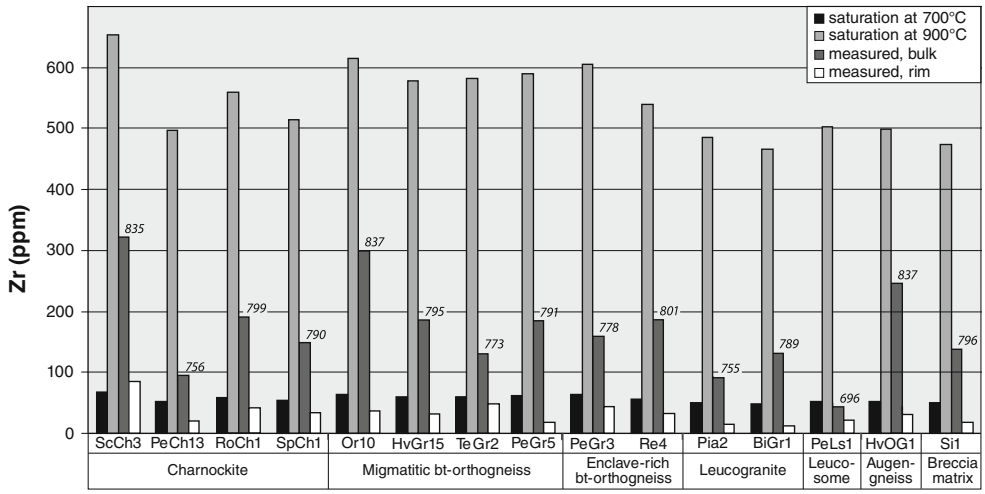

Fig. 11 Summary results of zircon dissolution calculation for the Gruf metagranitoids using the equation of Watson and Harrison (1983). The diagram displays the relationships between measured bulk Zr concentration, Zr concentrations saturating the granitic melts at 700 and 900°C and estimated Zr contents hosted in the 34- to 29-Ma outer zircon rims. At ultrahigh temperatures of 900°C as estimated for the formation of the Gruf charnockites and granulites (Galli et al. 2011), all the investigated melt compositions would be undersaturated in Zr with respect to zircon crystallisation. If such high-grade conditions were achieved during the Alpine metamorphism, dominantly Permian zircons would not be expected. Instead, estimated Zr contents in the Alpine zircon rims fit well the calculated Zr concentration that could be dissolved during melting at 700°C, suggesting that Alpine rim (re)crystallisation occurred during partial melting at upper amphibolite facies conditions of about 700°C, in accordance with thermobarometric P–T estimates for the Alpine Lepontine metamorphism in the Gruf Complex (Galli et al. 2012)

their Zr could have been dissolved in the parental melt. Accordingly, zircons could all have crystallised from the cooling charnockite melt. In support of this conclusion, xenocrystic cores are rare in the studied samples. They correspond to the few ages older than 280–260 Ma, and we take this latter age, obtained from the oscillatory cores that make up 70–80 vol% of the zircon grains, as that of the charnockite formation.

Zircon dissolution during Alpine remelting: age of migmatites

The homogeneity of volumetrically large zircon rims (50–55 vol%) in the leucosome sample (Fig. 5e) and in one of the migmatitic biotite-orthogneisses (35–40 vol% rim, sample TeGr2, Fig. 5b) indicates that in situ melting did not necessarily lead to oscillatory rims. Therefore, whether

rim formation is only fluid-assisted or associated with partial melting cannot be demonstrated. The temperatures of 720–740°C determined for Alpine metamorphism (Fig. 2, Galli et al. 2011) would lead to partial melting in granitic bulk compositions in the presence of aqueous fluids. Thus, fluid-assisted recrystallisation at the Alpine peak conditions is not feasible. The clear textural and petrological evidence for late deformation migmatisation thus leads to the conclusion that the 34- to 29-Ma zircon rims date this migmatisation. The degree of melting necessary to form such rims through crystallisation from a granitic melt of close-to-eutectic composition would be 10–20 vol%, which is broadly consistent with the degree of melting expected during metamorphism at 700–750°C.

Rims are oscillatory zoned in the enclave-rich biotite-orthogneiss and the magmatic breccia (Fig. 5c, g). The amount of Zr contained in these rims requires at least 20–30 vol% of melting (at 700°C). The field occurrence of these two lithologies suggests major movements of a granitic magma or crystal mushes (see Discussion below) at the time given by the age of these rims (31 and 32 Ma, respectively).

In conclusion, the Gruf Complex is composed of mostly Permian gneisses that suffered moderate Alpine migmatisation. These gneisses contain sheets of Permian charnockites, which in turn contain most of the granulites.

Significance of the Gruf ages in the Alpine context

Three main groups of ages have been recognised within the zircons separated from the metagranitoids of the Gruf Complex: (1) Cambro–Ordovician ~510–530 Ma and ~455–470 Ma; (2) Permian ~290–260 Ma, and (3) Oligocene ~34–29 Ma (Fig. 12).

Cambro–Ordovician xenocrysts

Concordant Cambrian (~513 Ma) and Ordovician (453 Ma) ages have been measured in cores of zircons from the enclave-rich biotite-orthogneisses (sample PeGr3). Similar ages have been reported from all over Western Europe, from Iberia (Lancelot and Allegret 1982; Sánchez-García et al. 2003) to the Bohemian Massif (Dostal et al. 2001; Friedl et al. 2004) through the Pyrenees (Delaperrière et al. 1994; Castiñeira et al. 2008), French Massif Central (Pin and Lancelot 1978; Melleton et al. 2010), Sardinia (Helbing and Tiepolo 2005; Oggiano et al. 2010) and the Alps (Sergeev and Steiger 1993, 1995; Bertrand and Leterrier 1997; Poller et al. 1997). These ages reflect magmatism at the end of the Cadomian orogeny and herald the continental break-up of Gondwana (Pin and Marini 1993; Von Raumer et al. 2002). The two ages from the same orthogneiss suggest a Cambrian precursor subsequently involved in remelting during Ordovician plutonism, a well-documented process (Alexandre 2007). The ca. 290 Ma zircon cores of sample Re4, the same orthogneiss as PeGr3, indicate additional remelting in Permian times.

Permian magmatic cores

Oscillatory and/or sector-zoned cores of zircons separated from charnockites, biotite-orthogneisses, leucogranites and the augengneiss yielded concordant Permian ages between 290 and 260 Ma. This finding is consistent with the zircon ages determined by Liati and Gebauer (2003) from a melanocratic, strongly restitic granulite boulder. The oscillatory zoned cores yielded 272 ± 4 Ma but were interpreted as dating a putative granitic precursor of the restitic granulites. Such an interpretation is at odds with the granulite chemistry, which requires a peraluminous metapelitic precursor (Galli et al. 2011). We thus take this 272 ± 4 Ma age as supporting our 282–260 Ma Permian age of the granulite metamorphism. The 32.7 ± 0.5 Ma milky rims of the 272 Ma zircons (Liati and Gebauer 2003) fit well with the age of Alpine migmatisation.

We interpret these ages as the time of emplacement of charnockite and granite magmas in the crust, consistent with worldwide magmatism at that time (Lorenz and Nicholls 1984; Veevers and Tewari 1995; Wilson et al. 2004). In Europe, the Permian magmatism is coeval with mafic underplating and lower crustal granitic intrusions that may partly derive from the granulitic lower crust; this event is associated with lithospheric thinning and transtensional collapse of the Variscan collisional orogen (Downes et al. 1990; Burg et al. 1994; Costa and Rey 1995; Schuster and Stüwe 2008). In the Alps, late Carboniferous-Permian intrusions are recognised in several places from the Ivrea Zone (Peressini et al. 2007) to the Eastern Alps (Eichhorn et al. 2000). The early Permian charnockites, orthogneisses and leucogranites dated in this work fit well into this picture, suggesting that the Gruf Complex constituted a piece of the European lower crust (Figs. 13 and 14a) at the same time (Hansmann et al. 2001; Henk et al. 1997; Tribuzio et al. 1999; Monjoie et al. 2007) and at similar conditions as for the Southern Alpine granulites of Ivrea (Barboza and Bergantz 2000), Malenco (Muntener et al. 2000), Sondalo (Braga et al. 2003) and Sesia (Lardeaux and Spalla 1991, Rebay and Spalla 2001) (Fig. 2).

The analysed zircon cores display a wide scattering of partly discordant Permo-Triassic ages as late as ca. 200 Ma (Figs. 6, 7, 8, 9). This feature is common in Variscan granitoids of the Central and Western Alps (Schaltegger 1990; Gebauer et al. 1997; Vavra and Schaltegger 1999). It is generally attributed to post-crystallisation thermal events

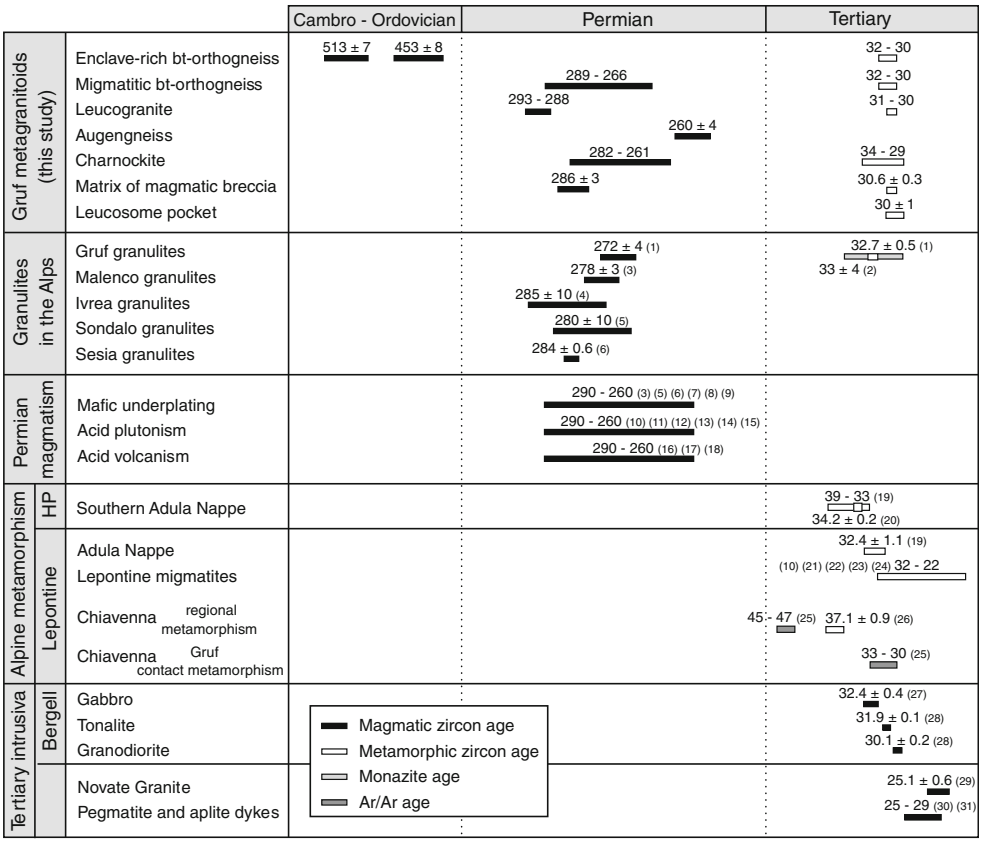

Fig. 12 Summary of calculated magmatic and metamorphic ages for the Gruf metagranitoids and comparison with geochronological data available for Permian granulites, Permian magmatism, Alpine metamorphism in the south- and south-eastern part of the Lepontine Dome and Tertiary intrusiva. References: (1) Liati and Gebauer (2003); (2) Schmitz et al. (2009); (3) Hansmann et al. (2001); (4) Henk et al. (1997); (5) Tribuzio et al. (1999); (6) Monjoie et al. (2007); (7) Pin (1986); (8) Quick et al. (2003); (9) Peressini et al. (2007); (10) Hänny et al. (1975); (11) Hunziker and Zingg (1980); (12) Pinarelli et al. (1988); (13) Boriani et al. (1990); (14) Bussy et al. (1998); (15) Marquer et al. (1998); (16) Barth et al. (1994); (17) De Capitani et al. (1994); (18) Schaltegger and Brack (2007); (19) Gebauer (1996); (20) Hermann et al. (2006); (21) Rubatto et al. (2009); (22) Berger et al. (2009); (23) Köppel et al. (1981); (24) Vance and O'Nions (1992); (25) Talerico (2000); (26) Liati et al. (2003); (27) Gregory et al. (2009); (28) Von Blanckenburg (1992); (29) Liati et al. (2000); (30) Romer et al. (1996); (31) Schärer et al. (1996)

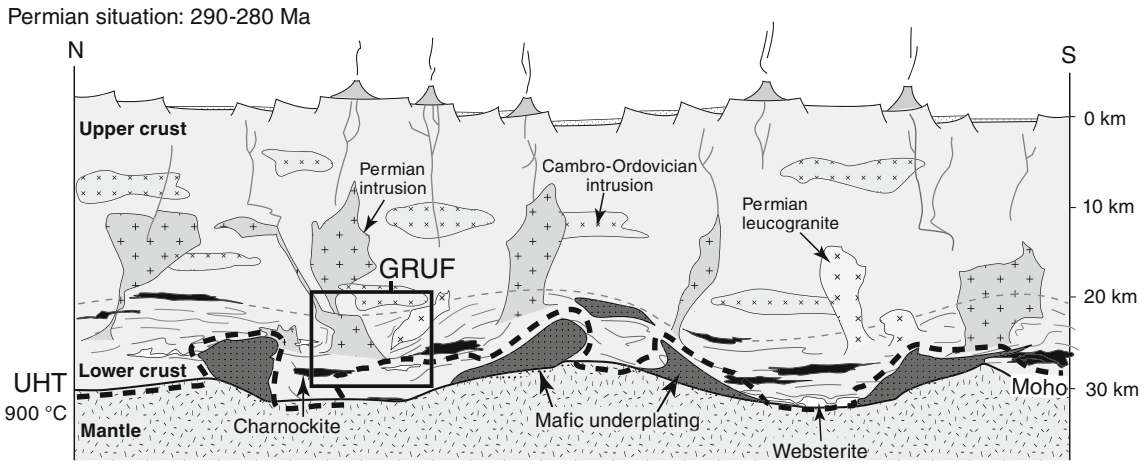

Fig. 13 Sketched petro-tectonic situation of the Gruf Complex during the Permian granulite facies event coeval with lithospheric thinning (see Discussion and References in text)

during renewed extension and magmatism in the late Permian to early Triassic (Schaltegger and Gebauer 1999), which signals opening of the Neo-Tethys Ocean (e.g. Ziegler 1993, Fig. 14b).

Early Oligocene metamorphic rims

Most analysed zircons have early Oligocene rims, dated between 34 and 29 Ma. These rims are coeval with the Alpine regional metamorphism (32–22 Ma in the southern and south-eastern Lepontine Dome, Hänny et al. 1975; Köppel et al. 1981; Vance and O'Nions 1992; Gebauer 1996; Berger et al. 2009; Rubatto et al. 2009) and the emplacement of the adjacent Bergell Pluton (33–30 Ma, Von Blanckenburg 1992; Oberli et al. 2004; Gregory et al. 2009). Field observations suggest that migmatisation at 720-740°C (Fig. 2) in the Gruf was contemporaneous with the Bergell pluton emplacement (Davidson et al. 1996; Berger et al. 1996; Galli et al. 2012).

The migmatisation event is also responsible for opx–cordierite symplectites around garnet and for cordierite rims around sapphirine, sillimanite, garnet or complex symplectites in both the granulite schlieren in the charnockites and in the strongly residual dark granulites (Galli et al. 2011). We further attribute the 33 ± 4.4 Ma age derived by Schmitz et al. (2009) through chemical U–Th–Pb dating of monazite to the Alpine migmatisation, although we concede that Schmitz et al. interpret this age as dating the granulite event. Nevertheless, a resetting of monazite during a migmatisation event protracted over 10 Ma (Rubatto et al. 2009) is feasible (Smith and Giletti 1997, Cherniak et al. 2004). The strongly variable degree of rim development from sample to sample and between grains of the same sample suggests a heterogeneous availability of metamorphic fluids that control the amount of anatectic melt. The oscillatory zoned rims demonstrate significant anatexis. Partial melting of granitic rocks produced leucocratic melts that locally intruded older rocks. Partial melting during Alpine metamorphism is further inferred from zircons extracted from the PeLs1 leucosome. These zircons partly (completely for one grain) re-equilibrated in the presence of melt at ca. 30 Ma.

Oscillatory zoned rims are prominent in the enclave-rich biotite-orthogneiss and the magmatic breccia. The amount of Zr contained in these rims requires but does not restrict melting to about 20–30 vol% (at 700°C). The viscosity of granitoid rocks molten to the extent of the rheological critical melt fraction of c. 30% is almost that of a granite melt (e.g. Arzi, 1978, Vigneresse et al. 1996). The magmatic breccia containing 5–50 vol% ultramafic enclaves is intrusive into the biotite-orthogneisses, and the oscillatory zircon rims suggest that it formed at 30.6 ± 0.3 Ma. Similarly, the oscillatory zircon rims of the enclave-rich orthogneiss at the contact Gruf–Chiavenna suggest a partially molten state of this granite sheet at 31–32 Ma (see also Fig. 3b). This corroborates our interpretation (Galli et al. 2012) that this sheet has accommodated most of the strain related to the ascent of the Gruf Complex along its northern boundary while the Bergell intrusion (30–32 Ma) was active at the southern and eastern limits of the Gruf.

Tectonic implications of the Permian granulite facies metamorphism

Since the charnockites represent melts formed at granulite facies conditions, their early Permian intrusion age dates the granulite event. Most of the granulites found in outcrops are indeed within the charnockites. Garnet diffusion modelling on the granulites reveals that within 20 Ma of the granulite facies garnet growth, these rocks have been cooled to less than 550–600°C (Galli et al. 2011). Hence, the Gruf granulites and charnockites have resided within the middle crust (or more shallow) between 240 Ma and the onset of prograde Alpine metamorphism (Fig. 14b, c). Garnet diffusion modelling shows that the 282–260 Ma granulite event is followed by cooling to less than 550–600°C within 20 Ma (Galli et al. 2011). All studied rocks record early Oligocene migmatisation. The UHT granulitic relicts found in the Gruf Complex are therefore polymetamorphic, polyorogenic rocks. They were therefore part of the lower crust formed and thermally re-equilibrated after the Variscan orogeny as identified in Western Europe (Fig. 14a).

It remains to bring the charnockites and granulites, formed at ≥900°C, into contact with the volumetrically dominant migmatitic gneisses and metasediments of the Gruf (Fig. 3b), which have not suffered through more than 700–750°C. Two possibilities are envisaged:

One considers the charnockites as intrusions originating in the lower crust and emplaced in amphibolite but not granulite grade paragneisses while post-Variscan granites intruded shallower crustal levels. Schlieren and boudins of granulites are enclaves of the lower crust in the charnockites. Not all granulites found in outcrops are enclosed by charnockites, but not all charnockites are necessarily preserved, as migmatisation may have completely destroyed opx. In this model, the charnockites, granites, and metasediments of the Gruf Complex would be involved in Alpine migmatisation as a mostly coherent block.

Alternatively, the charnockites and granulites of the Pangaea lower crust were introduced into the migmatitic gneisses and metasediments during the Alpine orogeny. In this model, the Gruf did not form a coherent mass since the Permian but only contains Permian lower crust and intrusions that have been partly exhumed during Triassic extension.

We follow previous tectonic models involving asymmetric extension of the European margin (e.g. Manatschal

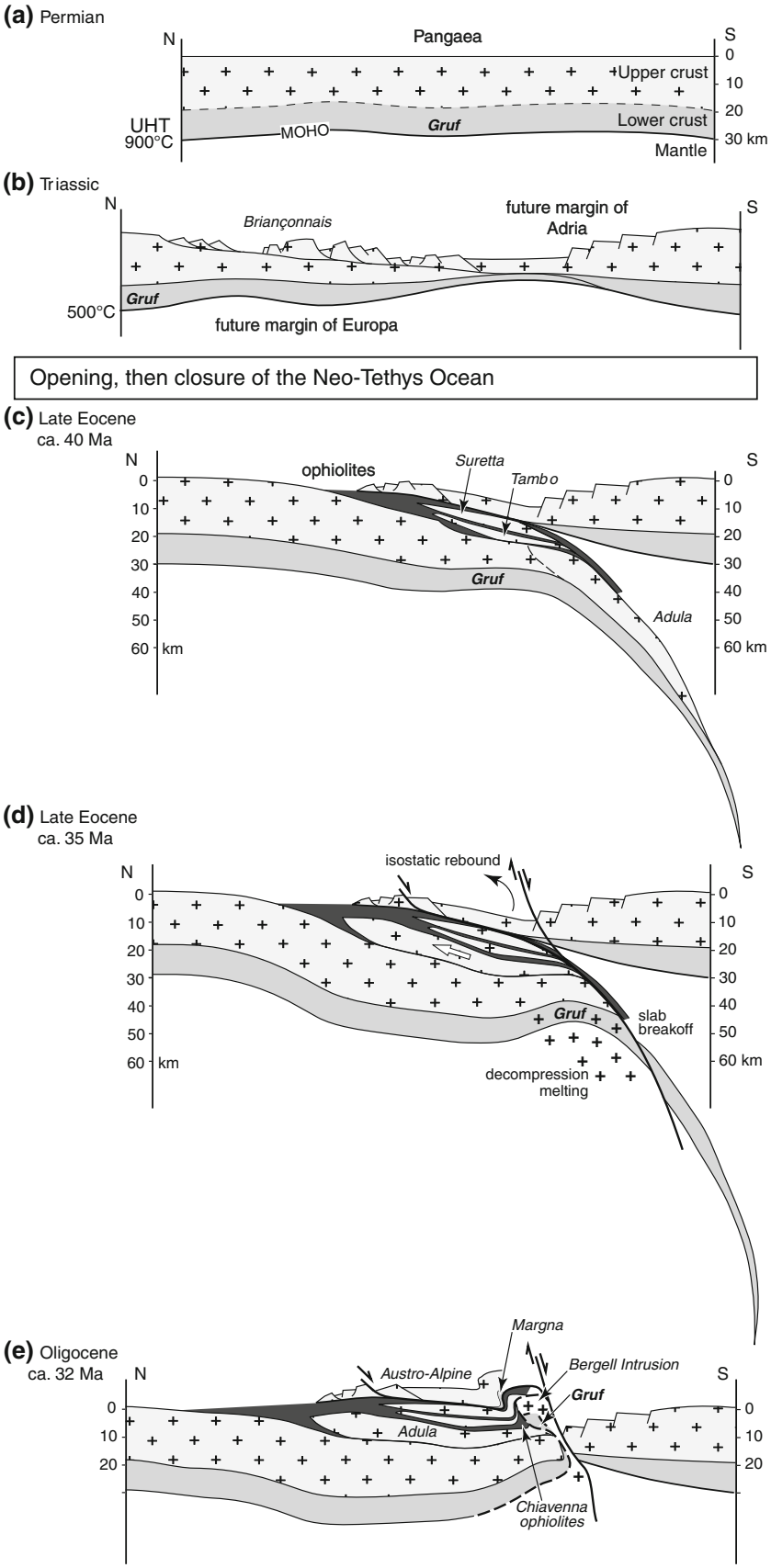

Fig. 14 Summarised tectonic evolution of the eastern Central Alps enabling the emplacement of the Gruf Complex in the context of late Eocene slab breakoff and subsequent, extensional roll-back of the European plate, which opened crustal space for the Bergell intrusion

et al. 2006) before opening (Fig. 14b) of the Tethys Ocean, which was accompanied by cooling and subsequent thermal subsidence of the European and Adrian margins. We also follow previous authors (e.g. Schmid et al. 1996; Froitzheim et al. 2003) in closing the Tethys Ocean by south-dipping subduction below the northern margin of Adria. We further follow the same models in subducting the European margin deep enough to produce eclogites that characterise the Adula Nappe (Fig. 14c). From that stage we refer to analogue (Chemenda et al. 2001) and numerical modelling (Gerya et al. 2008; Duretz et al. 2011). Buoyancy forces of the deeply buried continental crust overwhelm crustal strength and trigger upward extrusion of crustal segments such as Adula (Fig. 14d). Upward extrusion has important consequences: it thickens the orogenic system by addition of crustal slabs within the orogenic crust and it weakens the subducted lithosphere by removing crustal material delaminated from its lower crust and upper mantle. These two phenomena favour slab breakoff. The subsequent early Oligocene roll-back of the orogenic system, freed from slab pull, leads to rapid uplifting for isostatic reasons (Fig. 14d). This major event is consistent with the ascent of the Bergell Pluton at 32 Ma (Von Blanckenburg 1992) and the contemporaneous erosion climax attested by Oligocene deposits in the Molasse basin (Hay et al. 1992). Roll-back is a rotation that opens space for magma emplacement, hence for the mantle-derived Bergell Pluton in the Alpine crust. We contend that the Bergell magmas have dragged some of the lower crustal granulites and charnockites (Fig. 14e). Some of the volumetrically small granulitic chunks were mixed with migmatitic ortho- and paragneisses, perhaps as ductile inner part of the Bergell contact aureole. The buoyant, partially molten Gruf Complex was ascended towards upper levels with the Bergell Pluton (Fig. 14e). Exhumation of lower crustal blocks and migmatites next to buoyant plutons is well documented and reproduced in numerical models of magma intrusion (e.g. Best and Christiansen 2001; Gerya and Burg 2007). Numerical models tuned for the Bergell case should clarify this thermo-mechanical history.

Both interpretations are consistent with the absence of granulite facies assemblages in ultramafic, mafic and calcareous remnants of Mesozoic ophiolites within the Gruf (Schmid et al. 1996; Galli et al. 2012). In both models, the emplacement of the large mass of Gruf migmatitic gneisses would have produced the extreme temperature gradient of 70°C/km in the adjacent Chiavenna ophiolites.

Conclusions

1. The main part of the Gruf Complex is constituted by metagranitoids of Permian age formed between 290 and 260 Ma during post-Variscan extension and break-up of Pangea. These granitoids have intruded and assimilated the older Cambro–Ordovician crust with a peri-Gondwana, European signature.
2. Charnockitic magmatism and the formation of the sapphirine-bearing granulites occurred between 282 and 260 Ma and were part of the lower continental crust of Europe formed during post-Variscan extension.
3. During opening of the Neotethys, the Gruf lower crust remained part of the Northern (European) margin, while all other known Permian lower crust slices formed part of the Southern margin.
4. The dominant phase of Alpine metamorphism occurred between 34 and 29 Ma, inducing 10-30% partial melting of older lithologies. The Gruf is devoid of eclogites. Therefore, it escaped continental subduction during the Alpine orogeny.

Acknowledgments Three anonymous reviews helped clarifying several aspects of the paper. The authors were supported by the ETH Zurich.

References

Alexandre P (2007) U–Pb SIMS ages from the French Massif Central and implication for the pre-Variscan tectonic evolution in Western Europe. Comptes Rendus Geosci 339:613–621

Arzi AA (1978) Critical phenomena in the rheology of partially melted rocks. Tectonophysics 44:173–184

Barboza SA, Bergantz GW (2000) Metamorphism and anatexis in the mafic complex contact aureole, Ivrea Zone, northern Italy. J Petrol 41:1307–1327

Barth S, Oberli F, Meier M (1994) Th–Pb versus U–Pb isotope systematics in allanite from co-genetic rhyolite and granodiorite: implications for geochronology. Earth Planet Sci Lett 124:149–159

Berger A, Rosenberg C, Schmid SM (1996) Ascent, emplacement and exhumation of the Bergell pluton within the Southern Steep Belt of the Central Alps. Schweiz Mineral Petrogr Mitt 76:357–382

Berger A, Burri T, Alt-Epping P, Engi M (2008) Tectonically controlled fluid flow and water-assisted melting in the middle crust: an example from the Central Alps. Lithos 102:598–615

Berger A, Rosenberg C, Schaltegger U (2009) Stability and isotopic dating of monazite and allanite in partially molten rocks: examples from the Central Alps. Swiss J Geosci 102:15–29

Bertrand JM, Leterrier J (1997) Granïtoides d'âge Paléozoïque inférieur dans le socle de Vanoise méridionale: géochronologie U–Pb du métagranite del'Arpont (Alpes de Savoie France) C.R. Acad. Sciences Paris. Sci Terre Planet 325:839–844

Best MG, Christiansen EH (2001) Igneous petrology. Blackwell, Malden, p 458

Black LP, Kamo SL, Allen CM, Aleinikoff JN, Davis DW, Korsch RJ, Foudoulis C (2003) TEMORA 1: a new zircon standard for Phanerozoic U-Pb geochronology. Chem Geol 200:155–170

Boriani A, Burlini L, Sacchi R (1990) The Cossato–Mergozzo–Brissago Line and the Pogallo Line (Southern Alps, Northern Italy) and their relationships with the late-Hercynian magmatic and metamorphic events. Tectonophysics 182:92–102

Braga R, Callegari A, Messiga B, Ottolini L, Renna MR, Tribuzio R (2003) Origin of prismatine from the Sondalo granulites (Central Alps, northern Italy). Eur J Min 15:393–400

Bucher-Nurminen K, Droop G (1983) The metamorphic evolution of garnet-cordierite-sillimanite-gneisses of the Gruf-Complex, Eastern Pennine Alps. Contrib Mineral Petrol 84:215–227

Burg JP, Van den Driescsche J, Brun JP (1994) Syn- to post-thickening extension in the Variscan Belt of Western Europe: modes and structural consequences. Géol France 3:33–51

Burri T, Berger A, Engi M (2005) Tertiary migmatites in the Central Alps: regional distribution, field relations, conditions of formation, and tectonic implications. Schweiz Mineral Petrogr Mitt 85:215–232

Bussy F, Venturini G, Hunziker J, Martinotti G (1998) U–Pb ages of magmatic rocks of the western Austroalpine Dent-Blanche-Sesia Unit. Schweiz Mineral Petrogr Mitt 78:163–168

Castiñeira P, Navidad M, Liesa M, Carreras J, Casas JM (2008) U–Pb zircon ages (SHRIMP) for Cadomian and Early Ordovician magmatism in the Eastern Pyrenees: new insights into the pre-Variscan evolution of the northern Gondwana margin. Tectonophysics 461:228–239

Chemenda AI, Hurpin D, Tang JC, Stephan JF, Buffet G (2001) Impact of arc-continent collision on the conditions of burial and exhumation of UHP/LT rocks: experimental and numerical modelling. Tectonophysics 341:137–161

Cherniak DJ, Watson EB (2003) Diffusion in zircon. In: Hanchar JM, Hoskin PWO (eds) Reviews in mineralogy and geochemistry, 53, Zircon. Mineral Society of America, Washington, pp 113–143

Cherniak DJ, Watson EB, Grove M, Harrison TM (2004) Pb diffusion in monazite: a combined RBS/SIMS study. Geochim Cosmochim Acta 68:829–840

Compston W, Williams IS, Kirschvink JL, Zichao Z, Guogan M (1992) Zircon ages for the Early Cambrian time-scale. J Geol Soc Lond 149:171–184

Corfu F, Hanchar JM, Hoskin PWO, Kinny P (2003) Atlas of zircon textures. In: Hanchar JM, Hoskin PWO (eds) Reviews in mineralogy and geochemistry 53, Zircon. Mineral Society of America, Washington, pp 469–500

Cornelius HP (1916) Ein alpines Vorkommen von Sapphirin. Cbl. Mineral, pp 265–269

Costa S, Rey P (1995) Lower crustal rejuvenation and growth during post-thickening collapse: insights from a crustal cross section through a Variscan metamorphic core complex. Geology 23:905–908

Davidson C, Rosenberg C, Schmid SM (1996) Synmagmatic folding of the base of the Bergell pluton, Central Alps. Tectonophysics 265:213–238

De Capitani L, Delitalia MC, Liborio G, Mottana A, Rodeghiero F, Thöni M (1994) The granitoid rocks of Val Navazze, Val Torgola and Val di Rango (Val Trompia, Lombardy, Italy). Mem Sci Geol (Padova) 46:329–343

De Laeter JR, Kennedy AK (1998) A double focusing mass spectrometer for geochronology. Int J Mass Spectr 178:43–50

Delaperrière E, Saint-Blanquat M, Brunel M, Lancelot J (1994) Géochronologie U–Pb sur zircons et monazites dans le massif du Saint–Barthélémy (Pyrénées, France): discussion des âges des événements varisques et prévarisques. Bull Soc Géol France 165:101–112

Dostal J, Patocka F, Pin C (2001) Middle/Late Cambrian intracontinental rifting in the central West Sudetes, NE Bohemian Massif (Czech Republic): geochemistry and petrogenesis of the bimodal metavolcanic rocks. Geol J 36:1–17

Downes H, Dupuy C, Leyreloup AF (1990) Crustal evolution of the Hercynian belt of Western Europe: Evidence from lower-crustal granulitic xenoliths (French Massif Central). Chem Geol 83:209–231

Duretz T, Gerya TV, May DA (2011) Numerical modelling of spontaneous slab breakoff and subsequent topographic response. Tectonophys 502:244–256

Eichhorn R, Loth G, Höll R, Finger F, Schermaier A, Kennedy A (2000) Multistage Variscan magmatism in the central Tauern Window (Austria) unveiled by U/Pb SHRIMP zircon data. Contrib Mineral Petrol 139:418–435

Engi M, Bousquet R, Berger A (2004) Explanatory notes to the map: Metamorphic structure of the Alps. Central Alps. Mitt Österr Mineral Gesell 149:53–69

Frey M, Ferreiro Mählmann R (1999) Alpine metamorphism of the Central Alps. Schweiz Mineral Petrogr Mitt 79:135–154

Frey M, Hunziker JC, Frank W, Bocquet J, Dal Piaz GV, Jäger E, Niggli E (1974) Alpine metamorphism of the Alps. A review. Schweiz Mineral Petrogr Mitt 54:247–290

Friedl G, Finger F, Paquette JL, Von Quadt A, McNaughton NJ, Fletcher IR (2004) Pre-Variscan geological events in the Austrian part of the Bohemian Massif deduced from U–Pb zircon ages. Int J Earth Sci 93:802–823

Froitzheim N, Pleuger J, Roller S, Nagel T (2003) Exhumation of high- and ultrahigh-pressure metamorphic rocks by slab extraction. Geology 31:925–928

Frost RB, Frost CD, Hulsebosch TP, Swapp SM (2000) Origin of charnockites of the Louis Lake Batholith, Wind River Range, Wyoming. J Petrol 41:1759–1776

Galli A, Le Bayon B, Schmidt MW, Burg JP, Caddick MJ, Reusser E (2011) Granulites and charnockites of the Gruf Complex: evidence for Permian ultra-high temperature metamorphism in the Central Alps. Lithos 124:17–45

Galli A, Le Bayon B, Schmidt MW, Burg JP, Reusser E (2012) Tectonometamorphic history of the Gruf Complex (Central Alps): exhumation of a migmatitic complex associated with the Bergell pluton. Swiss J Geosci (submitted)

Gebauer D (1996) A P-T-t path for an (ultra?-) high-pressure ultramafic/mafic rock-association and its felsic country-rocks based on SHRIMP-dating of magmatic and metamorphic zircon domains. Example: Alpe Arami (Central Swiss Alps). In: Basu A, Hart SR (eds) Earth processes: reading the isotopic code. American Geophysics Union, Washington, DC, pp 309–328

Gebauer D, Schertl HP, Brix M, Schreyer W (1997) 35 Ma old ultrahigh-pressure metamorphism and evidence fro very rapid exhumation in the Dora Maira Massif, Western Alps. Lithos 41:5–24

Gerya TV, Burg JP (2007) Intrusion of ultramafic magmatic bodies into the continental crust: numerical simulation. Phy Earth Plan Int 160:124–142

Gerya TV, Perchuk LL, Burg JP (2008) Transient hot channels: perpetrating and regurgitating ultrahigh-pressure, high-temperature crust-mantle associations in collision belts. Lithos 103:236–256

Gregory C, McFarlane C, Hermann J, Rubatto D (2009) Tracing the evolution of calcalkaline magmas: in situ Sm-Nd isotope studies of accessory minerals in the Bergell Igneous Complex, Italy. Chem Geol 260:73–86

Hanchar JM, Miller CF (1993) Zircon zonation patterns as revealed by cathodoluminescence and backscattered electron images: implications for interpretation of complex crustal histories. Chem Geol 110:1–13

Hänny R, Grauert B, Soptrajanova G (1975) Paleozoic migmatites affected by high-grade Tertiary metamorphism in the Central Alps (Valle Bodengo, Italy). A geochronological study. Contrib Mineral Petrol 51:173–196

Hansmann W, Müntener O, Hermann J (2001) U–Pb zircon geochronology of a tholeitic intrusion and associated migmatites at a continental crust–mantle transition, Val Malenco, Italy. Schweiz Mineral Petrogr Mitt 81:239–255

Hay WW, Wold CN, Hezog JM (1992) Preliminary mass-balanced 3-D reconstructions of the Alps and surrounding areas during the miocene. Lect Notes in Earth Sci 41:99–110

Helbing H, Tiepolo M (2005) Age determination of Ordovician magmatism in NE Sardinia and its bearing on Variscan basement evolution. J Geol Soc Lond 162:689–700

Henk A, Franz L, Teufel S, Oncken O (1997) Magmatic underplating, extension, and crustal reequilibration: insights from a cross-section through the Ivrea Zone and Strona-Ceneri Zone, Northern Italy. J Geol 105:367–377

Hermann J, Rubatto D, Trommsdorff V (2006) Sub-solidus Oligocene zircon formation in garnet peridotite during fast decompression and fluid infiltration. Mineral Petrol 88:181–206

Hoskin PWO, Schaltegger U (2003) The composition of zircon and igneous and metamorphic petrogenesis. In: Hanchar JM, Hoskin PWO (eds) Reviews in mineralogy and geochemistry, 53, Zircon. Mineral Society of America, Washington, pp 27–62

Hunziker JC, Zingg A (1980) Lower Paleozoic amphibolite to granulite facies metamorphism in the Ivrea-Zone (Southern Alps–Northern Italy). Schweiz Mineral Petrogr Mitt 60:181–213

Kilpatrick JA, Ellis DJ (1992) C-type magmas: igneous charnockites and their extrusive equivalents. Transact Roy Soc Edinburgh 83:155–164

Köppel V, Günthert A, Grünenfelder M (1981) Patterns of U-Pb zircon and monazite ages in polymetamorphic units of the Swiss Alps. Schweiz Mineral Petrogr Mitt 61:97–119

Lancelot JR, Allegret A (1982) Radiochronologie U/Pb de l'Ortogneiss de Alter Pedroso (Alto lentejo) et évolution anteé-hercynienne de l'Europe occidentale. Neues Jahrberichten Mineral Monatsh 9:305–394

Lardeaux JM, Spalla MI (1991) From granulites to eclogites in the Sesia zone (Italian Western Alps): a record of opening and closure of the Piedmont ocean. J MMetam Geol 9:35–59

Larionov AN, Andreichev VA, Gee DG (2004) The Vendian alkaline igneous suite of northern Timan: ion microprobe U–Pb zircon ages of gabbros and syenite. In: Gee DG, Pease VL (eds) The Neoproterozoic Timanide Orogen of Eastern Baltica. Geological Society of London Members, vol 30, pp 69–74

Liati A, Gebauer D (2003) Geochronological constraints for the time of metamorphism in the Gruf Complex (Central Alps) and implications for the Adula-Cima Lunga nappe system. Schweiz Mineral Petrogr Mitt 83:159–172

Liati A, Gebauer D, Fanning CM (2000) U–Pb SHRIMP dating of zircon from the Novate granite (Bergell, Central Alps): evidence for Oligocene–Miocene magmatism, Jurassic/Cretaceous continental rifting and opening of the Valais trough. Schweiz Mineral Petrogr Mitt 80:305–316

Liati A, Gebauer D, Fanning CM (2003) The youngest basic oceanic magmatism in the Alps (Late Cretaceous; Chiavenna unit, Central Alps): geochronological constraints and geodynamic significance. Contrib Mineral Petrol 146:144–158

Lorenz V, Nicholls IA (1984) Plate and intraplate processes of Hercynian Europe during the Late Paleozoic. Tectonophysics 107:25–56

Ludwig KR (2005a) SQUID 1.12 A User's manual. A geochronological toolkit for Microsoft excel. Berkeley Geochronology Center Spec Pub, 22 p

Ludwig KR (2005b) User's manual for ISOPLOT/Ex 3.22. A geochronological toolkit for Microsoft excel. Berkeley Geochronology Center Spec Pub, 71 p

Marquer D, Challandes N, Schaltegger U (1998) Early Permian granitoid magmatism in Briançonnais terranes: Truzzo granite and Roffna rhyolite (Eastern Penninic nappes, Swiss and Italian Alps). Schweiz Mineral Petrogr Mitt 78:397–414

Mc Laren AC, Fitzgerald JD, Williams IS (1994) The microstructure of zircon and its influence on the age determination from Pb/U isotopic ratios measured by ion microprobe. Geoch Cosmo Acta 58:607–610

Melleton J, Cocherie A, Faure M, Rossi P (2010) Precambrian protoliths and Early Paleozoic magmatism in the French Massif Central: U–Pb data and the North Gondwana connection in the west European Variscan belt. Gondwana Res 17:13–25

Milnes AG, Pfiffner AO (1980) Tectonic evolution of the Central Alps in the cross section St. Gallen-Como. Eclog Geol Helv 73:619–633

Monjoie P, Bussy F, Schaltegger U, Mulch A, Lapierre H, Pfeifer HR (2007) Contrasting magma types and timing of intrusion in the Permian layered mafic complex of Mont Collon (Western Alps, Valais, Switzerland): evidence from U/Pb zircon and $^{40}Ar/^{39}Ar$ amphibole dating. Swiss J Geosci 100:125–135

Muntener O, Hermann J, Trommsdorff V (2000) Cooling history and exhumation of lower crustal granulite and upper mantle (Malenco, Eastern Central Alps). J Petrol 41:175–200

Nagel T, De Capitani C, Frey M (2002) Isograds and P-T evolution in the eastern Lepontine Alps (Graubünden, Switzerland). J Metam Geol 20:309–324

Niggli E, Niggli C (1965) Karten der Verbreitung einiger Mineralien der alpidischen Metamorphose in den Schweizer Alpen (Stilpnomelan, Alkali-Amphibol, Chloritoid, Staurolith, Disthen, Sillimanit). Eclog Geol Helv 58:335–368

Oberli F, Meier M, Berger A, Rosenberg C, Gieré R (2004) U-Th-Pb and $^{230}Th/^{238}U$ disequilibrium isotope systematics: precise accessory mineral chronology and melt evolution tracing in the Alpine Bergell intrusion. Geoch Cosmo Acta 68:2543–2560

Oggiano G, Gaggero L, Funedda A, Buzzi L, Tiepolo M (2010) Multiple early Paleozoic volcanic events at the northern Gondwana margin: U–Pb age evidence from the Southern Variscan branch (Sardinia, Italy). Gondwana Res 17:44–58

Oliver NHS, Bodorkos S, Nemchin AA, Kinny PD, Watt GR (1999) Relationships between Zircon U–Pb SHRIMP Ages and Leucosome Type in Migmatites of the Halls Creek Orogen, Western Australia. J Petrol 40:1553–1575

Paterson BA, Stephens WE, Rogers G, Williams IS, Hinton RW, Herd DA (1992) The nature of zircon inheritance in two granite plutons. Earth Sci 83:459–471

Peressini G, Quick JE, Sinigoi S, Hofmann AW, Fanning M (2007) Duration of a Large Mafic Intrusion and Heat Transfer in the Lower Crust: a SHRIMP U–Pb Zircon study in the Ivrea–Verbano Zone (Western Alps, Italy). J Petrol 48:1185–1218

Pin C (1986) Datation U–Pb sur zircons à 285 M.a. du complexe gabbro-dioritique du Val Sesia–Val Mastallone et âge tardi-hercynien du métamorphisme granulitique de la zone Ivrea–Verbano (Italie). Comptes Rend Ac Sci 303:827–830

Pin C, Lancelot JR (1978) Un exemple de magmatisme cambrien dans le Massif Central: les métadiorites quartziques intrusives dans la série de Lot. Bull Soc Géol France 20:203–208

Pin C, Marini F (1993) Early Ordovician continental brwak-up in Variscan Europe: Nd–Sr isotope and trace element evidence from bimodal igneous associations of the Southern Massif Central, France. Lithos 29:177–196

Pinarelli L, Del Moro A, Boriani A (1988) Rb–Sr geochronology of Lower Permian plutonism in Massiccio dei Laghi, Southern Alps (NW Italy). Rend Soc Ital Mineral Petrogr 43:411–428

Poller U, Liebetrau V, Todt W (1997) U–Pb single-zircon dating under cathodoluminescence control (CLC-method): application to polymetamorphic orthogneisses. Chem Geol 139:287–297

Quick JE, Sinigoi S, Snoke AW, Kalakay TJ, Mayer A, Peressini G (2003) Geologic map of the southern Ivrea-Verbano Zone, Northwestern Italy. Geologic Investigations Series, map I-2776 USGS, map + pamphlet, p 22

Rebay G, Spalla MI (2001) Emplacement at granulite facies conditions of the Sesia-Lanzo metagabbros: an early record of Permian rifting? Lithos 58:85–104

Romer RL, Schärer U, Steck A (1996) Alpine and pre-Alpine magmatism in the root-zone of the western Central Alps. Contrib Mineral Petrol 123:138–158

Rubatto D, Hermann J, Berger A, Engi M (2009) Protracted fluid-present melting during Barrovian metamorphism in the Central Alps. Contrib Mineral Petrol 158:703–722

Sánchez-García T, Bellido F, Quesada C (2003) Geodynamic setting and geochemical signatures of Cambrian–Ordovician rift-related igneous rocks (Ossa-Morena Zone, SW Iberia). Tectonophysics 365:233–255

Schaltegger U (1990) Post-magmatic resetting of Rb–Sr whole rock ages—a study in the Central Aar Granite (Central Alps, Switzerland). Geol Rund 79:709–724

Schaltegger U, Brack P (2007) Crustal-scale magmatic system during intracontinental strike-slip tectonics: U, Pb and Hf isotopic constraints from Permian magmatic rocks of the Siuthern Alps. Int J Earth Sci 96:1131–1151

Schaltegger U, Gebauer D (1999) Pre-Alpine geochronology of the Central, Western and Southern Alps. Schweiz Mineral Petrogr Mitt 79:79–88

Schärer U, Cosca M, Steck A, Hunziker J (1996) Termination of major ductile strike-slip shear and differential cooling along the Insubric line (Central Alps): U–Pb, Rb–Sr and $^{40}Ar/^{39}Ar$ ages of cross-cutting pegmatites. Earth Plan Sci Lett 142:331–351

Schmid SM, Pfiffner OA, Froitzheim N, Schönborn G, Kissling E (1996) Geophysical-geological transect and tectonic evolution of the Swiss-Italian Alps. Tectonics 15:1036–1064

Schmitz S, Möller A, Wilke M, Malzer W, Kannigiesser B, Bousquet R, Berger A, Schefer S (2009) Chemical U-Th-Pb dating of monazite by 3D-Micro X-ray fluorescence analysis with synchrotron radiation. Eur J Mineral 21:927–945

Schmutz H (1976) Der Mafitit-Ultramafitit-Komplex zwischen Chiavenna und Val Bondasca (Provinz Sondrio, Italien; Kanton Graubünden, Schweiz). Beitr Geol Karte Schweiz N.F. 149, 73 p

Schuster R, Stüwe K (2008) Permian metamorphic event in the Alps. Geology 36:603–606

Sergeev S, Steiger RH (1993) High-precision U–Pb single zircon dating of Variscan and Caledonian magmatic cycles in the Gotthard massif, Central Swiss Alps. Terra Nova Abstracts 5:394–395

Sergeev S, Steiger RH (1995) New estimate of emplacement and source ages of the acid gneisses constituting the pre-Alpine basement: single-zircon and zircon fragment U/Pb dating. Schweiz Mineral Petrogr Mitt 76:121–122

Smith HA, Giletti BJ (1997) Lead diffusion in monazite. Geoch Cosmo Acta 61:1047–1055

Stacey JS, Kramers JD (1975) Approximation of terrestrial lead isotope evolution by a two-stage model. Earth Planet Sci Lett 26:207–221

Steiger RH, Jäger E (1977) Subcommission on geochronology: convention on the use of decay constants in geo- and cosmochronology. Earth Planet Sci Lett 36:359–362

Stevens G, Clemens JD, Droop GTR (1997) Melt production during granulite-facies anatexis: experimental data from "primitive" metasedimentary protoliths. Contrib Mineral Petrol 128:352–370

Talerico C (2000) Petrological and chemical investigation of a metamorphosed oceanic crust-mantle section (Chiavenna, Bergell Alps). Ph.D. Thesis, ETH, Zurich, Nr. 13934

Tera F, Wasserburg GJ (1972) U-Th-Pb systematics in three Apollo 14 basalts and the problem of initial Pb in lunar rocks. Earth Plan Sci Lett 14:281–304

Todd CS, Engi M (1997) Metamorphic field gradients in the Central Alps. J Metam Geol 15:513–530

Tole MP (1985) The kinetics of dissolution of zircon ($ZrSiO_4$). Geoch Cosmo Acta 49:453–458

Tribuzio R, Thirlwall MF, Messiga B (1999) Petrology, mineral and isotope geochemistry of the Sondalo gabbroic complex (Central Alps, Northern Italy): implications for the origin of post-Variscan magmatism. Contrib Mineral Petrol 136:48–62

Trommsdorff V (1966) Progressive Metamorphose kieseliger Karbonatgesteine in den Zentralalpen zwischen Bernina und Simplon. Schweiz Mineral Petrogr Mitt 46:431–460

Vance D, O'Nions RK (1992) Prograde and retrograde thermal histories from the Central Swiss Alps. Earth Plan Sci Lett 114:113–129

Vavra G, Schaltegger U (1999) Post-granulite facies monazite growth and rejuvenation during Permian to Lower Jurassic thermal and fluid events in the Ivrea Zone (Southern Alps). Contrib Mineral Petrol 134:405–414

Veevers JJ, Tewari RC (1995) Permian-Carboniferous and Permian-Triassic magmatism in the rift zone bordering the Tethyan margin of southern Pangea. Geology 23:467–470

Vielzeuf D, Holloway JR (1988) Experimental determination of the fluid-absent melting relations in the politic system. Contrib Mineral Petrol 98:257–276

Vielzeuf D, Schmidt MW (2001) Melting relations inn hydrous systems revisited: Application to metapelites, metagreywackes, and metabasalts. Contrib Mineral Petrol 141:251–267

Vigneresse JL, Barbey P, Cuney M (1996) Rheological transitions during partial melting and crystallization with application to felsic magma segregation and transfer. J Petrol 37:1579–1600

Von Blanckenburg F (1992) Combined high-precision chronometry and geochemical tracing using accessory minerals: applied to the Central-Alpine Bergell intrusion (Central Europe). Chem Geol 100:19–40

Von Raumer JF, Stampfli GM, Borel G, Bussy F (2002) Organization of pre-Variscan basement areas at the north-Gondwanan margin. Int J Earth Sci 91:35–52

Watson EB (1979) Zircon saturation in felsic liquids: experimental results and applications to trace element geochemistry. Contrib Mineral Petrol 70:407–419

Watson EB (1996) Dissolution, growth and survival of zircons during crustal fusion: kinetic principles, geological models and implications for isotopic inheritance. Trans R Soc Edinburgh 87:43–56

Watson EB, Harrison TM (1983) Zircon saturation revisited: temperature and composition effects in a variety of crustal magma types. Earth Plan Sci Lett 64:295–304

Wenk E (1955) Eine Strukturkarte der Tessiner Alpen. Schweiz Mineral Petrogr Mitt 35:311–319

Wenk HR, Cornelius SB (1977) Geologischer Atlas der Schweiz, 1:25'000, Blatt Sciora. Publikationen Schweiz Geol Kommission

Wenk HR, Wenk E, Wallace JH (1974) Metamorphic mineral assemblages in pelitic rocks of the Bergell Alps. Schweiz Mineral Petrogr Mitt 54:507–554

Wetherill GV (1956) Discordant Uranium-Lead ages, I. Trans American Geoph Union 37:320–326

Wiedenbeck M, Alle P, Corfu F, Griffin WL, Meier M, Oberli F, Von Quadt A, Roddick JC, Spiegel W (1995) Three natural zircon standards for U-Th-Pb, Lu-Hf, trace element and REE analyses. Geostandards Newslett 19:1–23

Williams IS (1998) U-Th-Pb geochronology by ion microprobe. In: McKibben MA, Shanks WC, Ridley WI (eds) Applications of microanalytical techniques to understanding mineralizing processes. Reviews Economic Geology, vol 7, pp 1–35

Williams IS, Buick S, Cartwright I (1996) An extended episode of early Mesoproterozoic metamorphic fluid flow in the Reynolds Range, central Australia. Jour Metam Geol 14:29–47

Wilson M, Neumann ER, Davies GR, Timmerman MJ, Heeremans M, Larsen BT (2004) Permo-Carboniferous magmatism and rifting in Europe. Geol Soc Spec Publ 223:1–10

Ziegler PA (1993) Late Palaeozoic-Early Mesozoic plate reorganization: evolution and demise of the Variscan fold belt. In: Von Raumer JF, Neubauer F (eds) Pre-Mesozoic geology in the Alps. Springer, Berlin, pp 203–216